Journal of Rock Mechanics and Geotechnical Engineering 9 (2017) 1010–1030

Contents lists available at ScienceDirect

Journal of Rock Mechanics and Geotechnical Engineering

journal homepage: www.rockgeotech.org

Full Length Article

Testing and modeling of cyclically loaded rock anchors

Joar Tistel*, Gustav Grimstad, Gudmund Eiksund

Department of Civil and Transport Engineering, Faculty of Engineering, Science and Technology, Norwegian University of Science and Technology (NTNU), Trondheim, Norway

ARTICLE INFO

Article history:
Received 4 April 2017
Received in revised form
29 May 2017
Accepted 2 July 2017
Available online 10 November 2017

Keywords:
Rock anchor
Rock bolt
Bond-slip model
Cyclic loading
Empirical model
Laboratory testing
Bond degradation

ABSTRACT

The Norwegian Public Roads Administration (NPRA) is planning for an upgrade of the E39 highway route at the westcoast of Norway. Fixed links shall replace ferries at seven fjord crossings. Wide spans and large depths at the crossings combined with challenging subsea topography and environmental loads call for an extension of existing practice. A variety of bridge concepts are evaluated in the feasibility study. The structures will experience significant loads from deadweight, traffic and environment. Anchoring of these forces is thus one of the challenges met in the project. Large-size subsea rock anchors are considered a viable alternative. These can be used for anchoring of floating structures but also with the purpose of increasing capacity of fixed structures. This paper presents first a thorough study of factors affecting rock anchor bond capacity. Laboratory testing of rock anchors subjected to cyclic loading is thereafter presented. Finally, the paper presents a model predicting the capacity of a rock anchor segment, in terms of a ribbed bar, subjected to a cyclic load history. The research assumes a failure mode occurring in the interface between the rock anchor and the surrounding grout. The constitutive behavior of the bonding interface is investigated for anchors subjected to cyclic one-way tensile loads. The model utilizes the static bond capacity curve as a basis, defining the ultimate bond τ_{bu} and the slip s_1 at τ_{bu}. A limited number of input parameters are required to apply the model. The model defines the bond-slip behavior with the belonging rock anchor capacity depending on the cyclic load level ($\tau_{max\ cy}/\tau_{bu}$), the cyclic load ratio ($R = \tau_{min\ cy}/\tau_{max\ cy}$), and the number of load cycles (N). The constitutive model is intended to model short anchor lengths representing an incremental length of a complete rock anchor.

1. Introduction

The Norwegian Public Roads Administration (NPRA) is planning to upgrade the E39 coastal route in Norway, a distance of about 1100 km. Fixed links at seven fjord crossings along this route will replace ferry connections. The fjord widths range up to 5 km and the depths reach 1300 m. Large bridge structures will be required to cross the fjords. A variety of bridge concepts might be used, whereas the most successful is determined by the local metrics. Suspension bridges, submerged tunnels, fixed bridges, floating bridges and combinations of these structures are conceivable alternatives. Two alternative concepts are illustrated in Figs. 1 and 2.

Anchors for suspension bridge main cables, floating bridge abutments or anchoring of buoyancy forces from the submerged tunnel are one of the challenges related to these structures. The complexity of this subject is depending on the boundaries, offshore/onshore installation, load characteristics (size, static, cyclic), ground conditions among the others. Different alternatives may be used to anchor the loads: gravity based structures (GBS), suction piles, driven piles, drilled piles, rock anchors and so on. Howard et al. (2013) presented the deep water anchors designed to anchor the pontoons of the new Evergreen point floating bridge (Seattle, USA). Drilled shaft anchors, gravity anchors, and fluke anchors are used. Large gravity anchors are traditionally applied to anchor suspension bridge main cables when there is large depth to firm bedrock. The anchor block at the west side of Akahsi Kaikyo is a large cylindrical foundation constituting the following metrics: 75 m depth, 85 m diameter, 2.2 m thick retaining wall, constructed using a slurry trench method, backfilled with concrete inside the cylinder (Furuya et al., 1994).

Suspension bridge main cables are commonly fixed using “end-anchored” grouted rock anchors when rock is accessible. The “end anchors” are accessible through inspection tunnels. The Hardanger

* Corresponding author.
E-mail address: joar.tistel@ntnu.no (J. Tistel).
Peer review under responsibility of Institute of Rock and Soil Mechanics, Chinese Academy of Sciences.

https://doi.org/10.1016/j.jrmge.2017.07.005

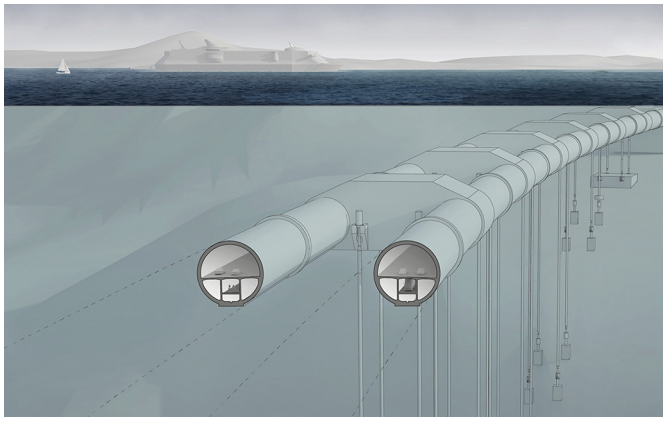

Fig. 1. Submerged floating tube bridge anchored to seabed, conceptual illustration (NPRA).

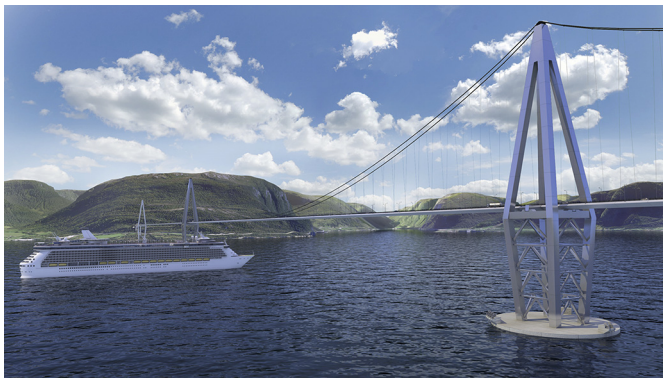

Fig. 2. Suspension bridge with floating towers, conceptual illustration (NPRA).

bridge used this method at both anchors whereas the Yi Sun-Sin bridge is designed with end anchor at one end only (Kim et al., 2012; NPRA, 2013). This method may be feasible for an onshore construction site. It might however be challenging for a deep-water offshore operation. The use of "traditional" large-scale rock anchors might therefore be an alternative. Offshore drilling vessels from the oil and gas industry might be used to drill and install rock anchors at large water depths. Both pre-stressed and passive anchors may be considered.

Experience with rock anchors of this size is elusive. Due to the nature of the loads, the poor availability for inspection and the possible severe consequences accompanying a failure, it is necessary to investigate the effects of cyclic loading combined with sustained loading (tension), creep, anchor-borehole ratio, anchor surface, failure mechanisms and grout properties amongst other factors.

There are in general four principal modes of failure of grouted anchors: (1) rock anchor tensile failure, (2) grout–anchor interface failure, (3) rock–grout interface failure, and (4) shear or uplift failure within the surrounding rock mass (Brown, 2015).

According to Benmokrane et al. (1995a), the failure tends to occur at the rock–grout interface in weak rocks and at the grout–tendon interface in strong rock provided that the tendon is sufficiently strong. The authors also state that the failure mechanism of anchors subjected to repeated loads may be different from those subjected to static loading. This might be caused by plastic strains in the anchor system, especially in the grout surrounding the bar/cable. Thus, when the anchors are subjected to repeated loads, they might suffer cumulative fatigue damage.

This paper investigates the rock anchor–grout interface bond strength reduction caused by cyclic loads. Other failure mechanisms are not evaluated within this paper. The research concerns passive rock anchors. The laboratory testing is performed on full-scale rock bolts to investigate the effects of repeated one-way cyclic loading in tension. The aim of the study is to assess the damage caused by cyclic loads and to establish a basis for prediction of corresponding rock anchor capacity. An empirical model predicting the behavior of incremental lengths of rock anchors subjected to cyclic load histories is presented in the paper. This model can be further developed to represent the full length of an infinitely long rock anchor in e.g. a finite element (FE) code.

A literature study is performed in order to shed light on factors affecting the rock anchor bond-slip relationship. Awareness of these factors and their influence on the holding capacity is crucial both in the laboratory work and in the development of a model describing the rock anchor behavior when subjected to cyclic loads. Research related to rebar in concrete is also evaluated. The study reveals few cross-references between the topic of bond-slip relations for rebar in concrete and grouted rock anchors. Research performed on the bond-slip relation between reinforcing bars in concrete is included in the study because the failure mechanism compares well to that of a grouted rock bolt given similar boundary conditions. The main findings from the literature study are summarized and presented within this paper.

2. Factors influencing bond-slip relationship

The topic of load transfer capability of rock anchors has been investigated in several publications. Standards and codes recommend an average (uniform) bond stress to be used for the complete anchored length (e.g. Brown, 2015). Measurement and theory show nevertheless varying mobilized shear stress along the anchor interface with relative slip between the steel tendon and the surrounding grout. In order to more accurately model the rock anchor capacity with anchored length, it is common to apply bond-slip curves to modeling the locally mobilized shear stress with relative slip between anchor and surrounding grout (Ma et al., 2016). The values of the bond and the corresponding slip depend on several factors, including not only physical factors related to the materials used, but also testing procedures and confinement of the grout surrounding the rock bolt.

Rock anchor bond degradation caused by cyclic loading is an important topic in the context of foundations relying on rock anchors. The consequences of failure in rock anchors might be severe, depending on the utilization of these structures. Only a limited number of data are published within the topic of cyclic degradation of rock anchor capacity caused by cyclic loading. There are apparently more information available with respect to cyclically loaded reinforcing bars in concrete than that about cyclically loaded rock anchors.

Theories and experimental data concerning pullout testing of reinforcing bars in concrete under monotonic and cyclic loads are investigated within this study. Main factors affecting the bond along a grouted rock anchor are presented in the following.

2.1. Length of bar for definition of local bond-slip relation

Several studies, both on rebar in concrete and on rock anchors, concern the local bond-slip relation. In order to isolate the local bond-slip relation from an average curve representing the complete anchor length, only a limited length of the anchor shall be

assessed. A literature study indicates that different lengths are used for this purpose.

The anchor–grout interface bond, or shear stress with slip relation, was studied by Benmokrane et al. (1995b). The local bond-slip relation was found by testing an incremental length of a grouted anchor. A length increment of 4 times the bar diameter was used to assess the constitutive relationship of the interfacial bond and the bolt slip. Rehm and Eligehausen (1979) used an anchored length of 3 times the bar diameter (rebar), and Hyett et al. (1992) used a length of 15–20 times the tendon diameter to study the effect of rock mass confinement on cable bolt bond.

When the anchored length is sufficiently short, the shear bond stress is uniformly distributed along the bolt-grout interface. RILEM (1994) recommended an anchored length of 5 times the bar diameter.

2.2. Effect of grout properties

There are mainly two different grout or mortar types being used: cement-based grout and resin grout. The grout shall provide required bond and protect the rock anchor from corrosion. Resin grouts are more plastic than cement grouts and can develop higher ultimate strengths, but the long-term performance is not yet fully documented. Yahia et al. (1998) reported that a number of failures occurred for submerged anchors installed with polyester resin grouts. Inspection revealed that the underwater-cast resin grout was soft and could be easily removed from the anchor by hand.

Kılıc et al. (2002) concluded that the bolt capacity depends basically on the mechanical properties of the grout materials which can be changed by water-cement ratio, mixing time, additives, and curing time. The following conclusions were drawn: (1) Optimum water-cement ratio was found to be in the range of 0.34–0.4; (2) increasing curing time increased the bolt bond strength, and (3) the mortar had to be well mixed. Benmokrane et al. (1995b) reported pullout tests on stranded cables and threaded bars with different anchored lengths. Different cement-based grouts with and without additives were tested using standard test procedures. The influence of water-cement ratio as well as different additives on the physical and mechanical properties of cement grouts was studied. The introduction of aluminum-based silica fume and sand to the standard grout appeared to improve the bond strength characteristics.

According to Lotsberg et al. (2011), the fatigue capacity of concrete in water is reduced when the concrete is subjected to cyclic stress ranges in compression. Dallyn et al. (2015) experimentally concluded that the *S-N* curve for grouted connections should be reduced by a factor of 0.8 compared to the in-air curve, where *S* is the stress, and *N* is the number of load cycles. Yahia et al. (1998) reported that underwater-cast anchors have lower pullout capacity than dry-cast anchors, and that the difference in capacity can be reduced by using grout with a high washout resistance.

Applying rock anchors with a deformed surface, e.g. a ribbed surface, weld beds or similar, will mobilize the compressive strength in the surrounding grout. Previous research on rebar pullout capacity in concrete has shown a strong correlation between pullout capacity and compression strength in concrete, which is also reflected in model code 1990 (CEB, 1991). Applying *S-N* relations similar to those suggested for concrete (e.g. Aas-Jakobsen, 1970) may therefore be relevant for grouted rock anchors (with deformed surface) subjected to load cycles. The stress fatigue life (*S-N*) expression, defined by Aas-Jakobsen (1970), is commonly used to describe the behavior of concrete subjected to cyclic loads:

$$\frac{S_{\max}}{f_c} = 1 - (1 - R)\beta \log_{10} N \tag{1}$$

where f_c is the static strength in compression; N is the fatigue life (or number of load cycles); β is a material parameter; and R is the stress ratio, $R = S_{\min}/S_{\max}$, $S_{\min}$ and $S_{\max}$ are the minimum and maximum stresses, respectively. This model does however not include the effect of load frequency. The equation suggested by Zhang et al. (1996) seeks to expand Eq. (1) by including the effect of load frequency:

$$\frac{S_{\max}}{f_c} = \left(ab_z^{-\log_{10} f} + c\right)[1 - (1 - R)\beta \log_{10} N] \tag{2}$$

where a, b_z and c are the curve parameters fitting to the laboratory test results; and f is the loading frequency. Studies by the same author show that the fatigue life is somewhat constant if the frequency is in the range of 1–10 Hz. The fatigue life decreased however if the loading frequency was decreased to 0.1 Hz. The effect of loading rate and creep should therefore also be considered in a model.

2.3. Time effects

Long-term creep may affect the behavior of passive or prestressed rock anchors. Creep may occur in the rock, grout or steel material and may reduce the anchor design life. Benmokrane and Ballivy (1991) performed a five-year study on prestressed anchors in sound rock. The study revealed two phases: the first phase lasting for about six months where the losses in load are rapid, followed by the second phase where the losses are slower and a uniform rate of loss is recorded. The major part of the loss in load is attributed to relaxation in the anchor steel. The authors also concluded that in the case of a weak rock, the contribution from the rock mass may also be significant. Re-stressing of anchors may reduce the subsequent losses of load, followed by grouting of the free part of the anchor to create an efficient casing against corrosion.

Rehm and Eligehausen (1979) compared reinforcing bars subjected to cyclic loads to specimens subjected to sustained loads. Sustained loads were applied on bars at similar load level as the cyclic load level. The results show that sustained and cyclic loads will have the same effect on the anchor in terms of redistribution of forces along the anchor length. Cyclic loads are thus considered a time accelerator. According to the authors, similar behavior is found for creep tests with unreinforced concrete specimens.

2.4. Anchor system stiffness properties

The ratio of the elastic modulus of the steelbar to that of grout (or rock) is found to have an important influence on the distribution of elastic shear stresses along the embedment length (Brown, 2015). The relative displacement between the anchor and surrounding grout will vary along the anchor length and depend on the stiffness ratio, $E_{\text{anchor}}/E_{\text{grout}}$. As the ratio increases in softer grouts and rocks, the stress distribution becomes more closely uniform. This means that the mobilized shear will vary accordingly. Where the deformations are very small, the resistance is developed primarily in adhesion and, with tension anchors under working load conditions, this will occur near the lower end of the fixed anchor length. At the upper end of the fixed anchor length, the relative displacements are greater due to the elastic stretch of the bar, then friction and perhaps interlocking effects will also apply. Where a frictional type of resistance is developed, its value depends on the degree of confinement provided by the grout column (Hanna, 1982).

Yazici and Kaiser (1992) presented a conceptual model explaining the development of the bond strength for cable bolts. If the ratio between rock stiffness and grout stiffness is large, there will be good confinement conditions, and the radial stress at the bar–grout interface might increase with increasing mobilization.

2.5. Borehole diameter and bar diameter

Yazici and Kaiser (1992) presented a model for fully grouted cable bolts. A sensitivity study presented in their paper shows a decreasing bond strength along the anchor length with increasing borehole diameter. They also suggested to use small boreholes for stiff rocks or undisturbed rock volumes.

Gómez et al. (2005) found that for micropile inserts grouted inside a borehole pre-drilled through a concrete mass, the diameter of the hole appears to have a significant influence on the average bond strength that can be achieved. The results suggest that, for a constant insert diameter, the average bond strength decreases with increasing borehole size. The reduction is explained by the relatively low Young's modulus in grout compared to that of concrete. This conclusion contradicts nevertheless the finding made by Yazici and Kaiser (1992).

Ivanović and Neilson (2009) commented on the importance of borehole to bar diameter ratio in pullout tests, and compared their results with those of Benmokrane et al. (1995a). For a larger borehole to bar diameter ratio, the tendency is that the failure will occur at the bar–grout interface. This is caused by a reduction in the shear stress at the periphery of a larger diameter borehole. Thus, the borehole to bar diameter ratio may determine the rock anchor failure mode.

2.6. Failure mode and confinement

Monotonic load tests performed on threaded steelbars (reinforcing bar in concrete) show two typical types of bond failures (ACI, 1992):

(1) The first is a direct pullout of the bar, which occurs when ample confinement is provided to the bar. The concrete immediately surrounding the bar fails due to the shearing of the concrete between the ribs. Pullout failures depend primarily on the concrete strength and the pattern and geometry of the ribs.
(2) The second type of failure is a splitting of the concrete cover when the cover or confinement is insufficient to obtain a pullout failure. The transfer of stress from the steelbars to the surrounding concrete is dependent on chemical adhesion, friction, and mechanical interlocking between the ribs of steelbars and concrete.

Hyett et al. (1992) conducted a laboratory and field program to investigate the major factors influencing the bond capacity of grouted cable bolts in rock. Their results indicated that the cable bolt capacity most critically depends on cement properties, embedment length and radial confinement acting on the outer surface of the cement annulus. The confinement was measured using "split-pipe" tests in laboratory, and surface tests on granite, limestone and shale in the field. As the degree of radial confinement increased, the failure mechanism changed from radial fracturing and lateral displacement of the grout annulus under low confinement, to shearing of the cement flutes and pullout along a cylindrical frictional surface under high confinement.

According to Kaiser et al. (1992), the bond strength of fully grouted cable bolts is primarily frictional and depends on the pressure at the cable–grout interface. They presented a study on the effect of stress change on the bond strength. Kılıc et al. (2002) performed laboratory tests to evaluate the shear strength effect on the bond strength of the bolt-grout interface of a threaded bar. According to the authors, the test results support the theory that the bond strength of fully cement-grouted rock bolts is primarily frictional and depends on the shear strength at the bolt-grout or grout–rock interface. The bolt capacity is consequently sensitive to stress change in rock mass, especially if the rock is soft. With respect to failure mechanism, Kılıc et al. (2002) concluded that the cracking of the grout is affected by the field stress change. Stress increases enhance the splitting resistance whereas stress decrease may crack the grout before dilation starts and the latter may lead to much lower cable bond capacities.

Application of expanding mortar may contribute to good confinement conditions. Rock anchor tests performed by Benmokrane et al. (1995a) failed using pullout failure mode. They used type I Portland cement including an expansive agent (aluminum powder) added at a ratio of 0.005% cement by weight.

2.7. Rock anchor surface

Kılıc et al. (2003) presented experimental results obtained from the direct pullout tests using different types of rock bolts having different shapes of ribs, including smooth surface bars, ribbed bars, single conical ribbed bars, double conical ribbed bars and triple conical ribbed bars. The results reveal a significant difference in pullout capacity compared with deformed and smooth bar surfaces. They concluded that the failure mechanism of the conical ribbed rock bolt is different from that of conventional one because the conical rib can provide more resistance due to wedging effect.

Model code 1990 (CEB, 1991) recommended the maximum values for smooth surface bond strength equal to $0.3\sqrt{f_c}$ for good bond conditions, and $0.15\sqrt{f_c}$ for poor bond conditions. For ribbed bars (e.g. threaded steelbars), the maximum recommended bond strength varies from $\sqrt{f_c}$ to $2.5\sqrt{f_c}$, depending on bond and confinement conditions.

The difference in terms of load transfer mechanism between stranded cables and threaded bars was investigated by Benmokrane et al. (1995b). The apparent average values of ultimate shear bond stress at the anchor–grout interface of stranded cables were generally one-third of the threaded bar values.

2.8. Bond strength and cyclic loads

Ballivy et al. (1988) performed repeated loading tests on laboratory scale passive anchors (cement grouted in concrete cylinder). The results indicate that the load amplitude and the upper/lower levels of load have a significant effect on the anchor service life or the number of repeated loadings at failure. This is in alignment with the findings from experimental tests on reinforcing bars in concrete (e.g. ACI, 1992). Furthermore, the upper-level repeated load less than 25% of the ultimate static load was reported to have no effect on the anchors at failure. Anchors subjected to an upper-level repeated load ($\tau_{max\ cy}$) greater than 70% of the ultimate static load failed only after a certain number of cycles, typically less than 100. When anchors were subjected to intermediate loading amplitude with the upper-level load ranging from 25% to 65% of the ultimate static load, negative effects developed on the load holding capacity and displacement at the anchor head.

Benmokrane et al. (1995a) presented the results of full-scale repeated loading tests performed on three prestressed and six passive rock anchors grouted to various lengths in a rock mass. The results from pullout tests on passive anchors subjected to repeated and static loads indicated that anchor failures were induced by shearing failure at the grout–anchor interface. Different levels and

amplitudes of one-way cyclic loads (in tension), ranging from 10% to 170% of the initial prestress load and from 10% to 73% of the ultimate static load were applied to prestressed and passive anchors, respectively. The study concluded that anchors subjected to repeated loadings have the same service life as those only subjected to static loading, provided that the applied repeated loads are less than the initial prestress loads for prestressed anchors, or less than 30% of the ultimate static loads for passive anchors. The authors also suggested that grouted anchors subjected to repeated loadings should be prestressed to loads greater than any likely load fluctuation, and the design capacity of the anchors should be 70% of the static load holding capacity.

Several research studies were published on the topic of cyclic degradation of bond between reinforcing bars in surrounding concrete. Ciampi et al. (1981), Eligehausen et al. (1981), ACI (1999), and Verderame et al. (2009a) presented studies and recommendations on modeling of rebar subjected to cyclic loads. There should apparently be parallels between the rebar-concrete and rock anchor (bar)-grout interface behaviors, especially if the rock anchor compares well to a deformed reinforcing bar. Furthermore, the effect of repeated loading on slip and bond strength of deformed bars compares well to the characteristics of the material behaviors (deformation and failure) of unreinforced concrete subjected to repeated loading in compression (Rehm and Eligehausen, 1979). The bond strength under cyclic loads is therefore to a large degree controlled by the surrounding grout material.

Rehm and Eligehausen (1979) found that if no fatigue failure occurs, a repeated load has only an influence on the bond behavior under service load. The increase of slip between steel and concrete causes a decrease of the local bond stiffness. The result is a redistribution of the forces along the anchor length which can also be expected under a sustained load of the same magnitude (i.e. creep). This was also verified in studies published by Oh and Kim (2007). Eligehausen et al. (1981) loaded a rebar (in concrete) monotonically to an arbitrary slip value, followed by cycling up to 10 times between this slip value and a slip value corresponding to a load equal to zero. The bar was thereafter loaded monotonically to increasing slip values. The monotonic (static) envelope was, for all practical purposes, reached again and followed thereafter.

2.9. Bond-slip models for monotonic testing

The static capacity of rock anchor is a basis in the assessment of damage or slip caused by cyclic loading action. CEB (1991) presented a local bond stress-slip model for monotonic loading of rebar in concrete. This model is basically identical to the model proposed by Eligehausen et al. (1981). According to Verderame et al. (2009b), this is also the model which best fits the experimental bond stress–slip behavior for reinforcing bars. The shape of the bond-slip curves varies, depending on the mass (concrete) surrounding the bar, the confinement, the surface of the bar and several other factors. Benmokrane et al. (1995b) suggested a tri-linear bond-slip curve to be used for determination of rock anchor capacity. This tri-linear curve is commonly used for rock bolt pullout capacity calculations. The two approaches are presented in Fig. 3a and b.

Bond-slip models for reinforcing bars in concrete and rock anchors should be comparable as long as the rock anchor constitutes a threaded steelbar grouted into a borehole, and if slip at the bar–grout interface is the governing failure mode.

Model code 1990 (CEB, 1991) defined the bond–slip relationship, intended for reinforcing bars in concrete, as follows:

$$\tau = \begin{cases} \tau_{bu}(s/s_1)^{\alpha} & (0 \le s \le s_1) \\ \tau_{bu} & (s_1 < s \le s_2) \\ \tau_{bu} - \left(\tau_{bu} - \tau_f\right)\dfrac{s - s_2}{s_3 - s_2} & (s_2 < s \le s_3) \\ \tau_f & (s > s_3) \end{cases} \tag{3}$$

where τ is the shear bond stress at anchor–grout interface, s is the slip between anchor and grout, τ_{bu} is the ultimate (or peak) bond capacity, and τ_f is the residual bond capacity.

The tri-linear curve defined by Benmokrane et al. (1995b) simply consists of three linear curves defined by

$$\tau = ms + n \tag{4}$$

The coefficients m and n for the three stages of shear bond stress-slip relation are given as

$$m = m_1 = \frac{\tau_{bu}}{s_1},\ n = 0 \quad (0 \le s \le s_1) \tag{5}$$

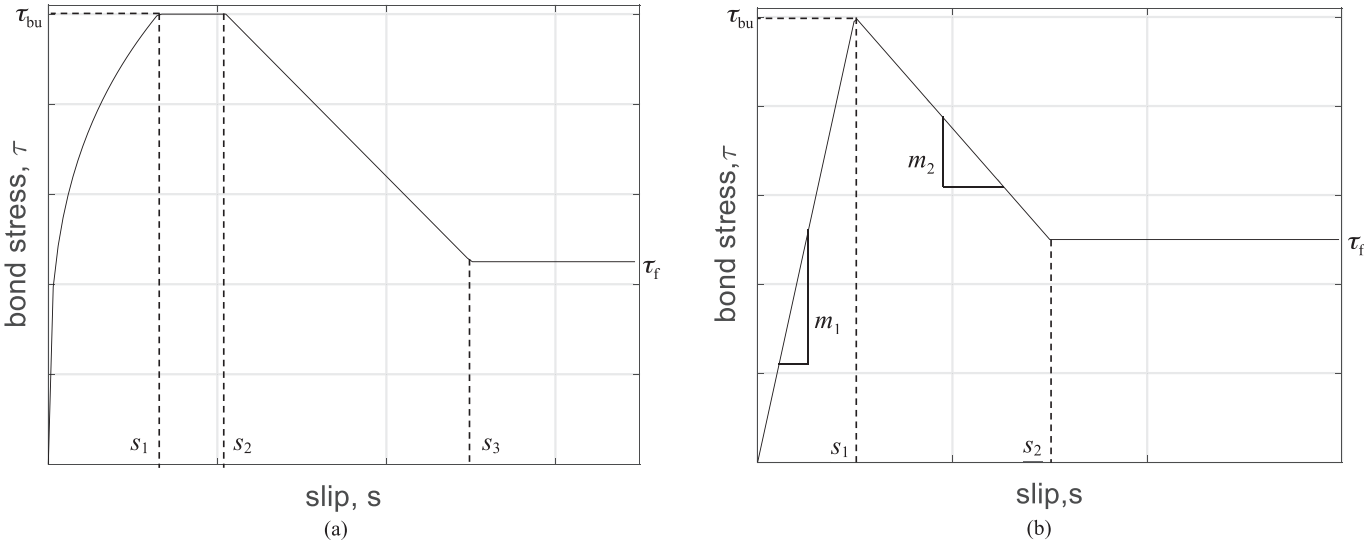

Fig. 3. (a) Bond-slip curve based on CEB (1991), and (b) tri-linear bond-slip curve defined by Benmokane et al. (1995b).

$$m = m_2 = \frac{\tau_{bu} - \tau_f}{s_1 - s_2},\ n = \frac{\tau_f s_1 - \tau_{bu} s_2}{s_1 - s_2} \quad (s_1 < s \le s_2) \tag{6}$$

$$m = 0,\ n = \tau_f \quad (s > s_2) \tag{7}$$

3. Experimental research

3.1. Purpose

The purpose of the experimental study is to provide a basis for the development of a model describing the progressive failure mechanism of a rock anchor subjected to cyclic loads. The constitutive relation between bond and slip at the bar–grout interface for bars subjected to cyclic loads at different load levels is addressed. The model shall account for the local bond stresses and associated damage caused by cyclic loads. A progressive failure mechanism can thus be modeled, given a load history input. The study seeks to develop general models for local slip (s) as a function of number of cycles per slip (dN/ds) at pre-defined load levels. Previous studies mainly describe relations between slip and number of cycles for slip below s_1 (slip at ultimate bond τ_{bu}) (Rehm and Eligehausen, 1979; Fib, 2000; Oh and Kim, 2007). These relations appear as linear curves in a double logarithmic plot. The relations are however inappropriate for slip beyond s_1. The slip vs. number of cycles beyond s_1 is crucial in the development of a strain compatible model.

The progressive failure mechanism at the bar–grout interface is illustrated in Fig. 4. The mobilized bond stresses move inwards with increasing number of load cycles. Studying the bar increment No. 9, it can be seen that the slip (s) at the first loading is less than s_1, implying that the ultimate bond stress, τ_{bu}, is not yet reached. At points B and C, additional slip is induced by N load cycles, and corresponding bond stress capacity is shown in the upper Fig. 4. At point D, the slip has passed the slip at peak bond stress, s_1. The maximum bond stress is reduced correspondingly. For a sufficiently large slip, the maximum bond stress will be reduced to the friction capacity τ_f.

3.2. Experimental test set-up

The experimental program includes a total of 47 grouted rock anchors. For each anchored length, both static pullout and cyclic tests are executed. Static pullout tests are performed for a minimum of two anchors with equal anchored length and the results are used as a reference for the static capacity for the given anchored length.

The anchors consist of ribbed steelbars and are installed in predrilled 50 mm boreholes in a cubic 1 m × 1 m × 1 m concrete block. The compressive strength of the concrete is 90 MPa. The boreholes are drilled by use of rotary drilling equipment. The center distance between the boreholes is approximately 150 mm. The purpose of the test program is to investigate the bond strength between the steelbar and the grout. A relatively large borehole diameter distributes the pull force to a larger area at the grout–borehole interface, and thereby minimizes the probability of slip in this area. A large diameter also allows for a certain correction of the verticality of the steelbar during installation.

The holes are drilled to about 400 mm depth and filled with grout prior to installing the bars. The bars are installed in a frame with the aim of maintaining the accurate vertical position of the bar during curing. Fig. 5 presents the concrete block and grouted steelbars.

The threaded steelbars are anchored into the concrete block by use of a cement-based grout, Mapei Nonset 50. This is an expanding

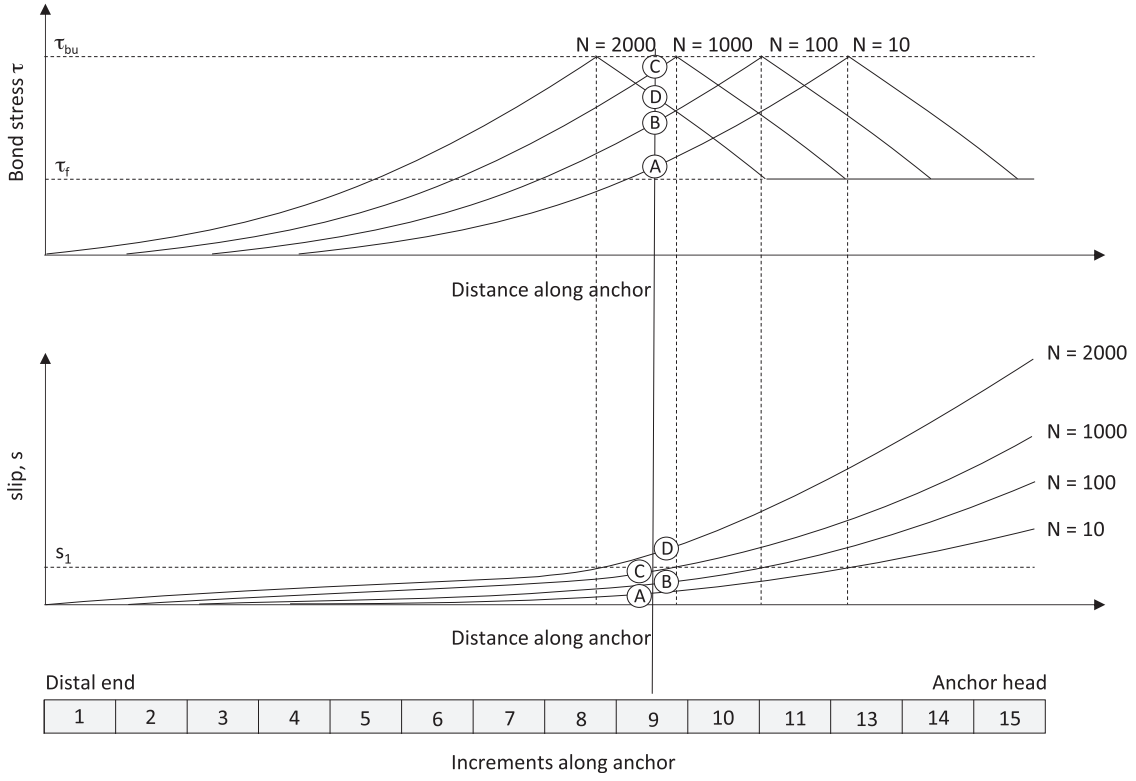

Fig. 4. Bond stress along anchor–grout interface. Element No.15 located at anchor head (at load application point). Principal sketch showing progressive failure mechanism with increasing number of load cycles.

Fig. 5. Threaded steelbars installed in concrete block.

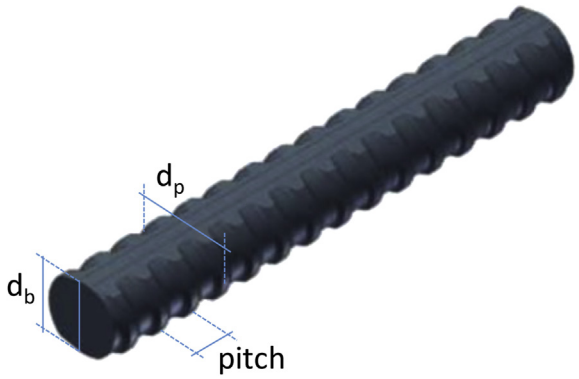

Fig. 6. Geometry of steelbar.

mortar for rock bolt grouting. Nonset 50 is a thixotropic cement-based, non-settling dry mortar, which expands 1%–3% before setting. The mortar is composed of Portland cement, with expanding, plasticizing and stabilizing additives and maximum diameter of additives, D_{max}, equal to 0.2 mm. The water-cement ratio is 0.4. Compression test specimens are casted and stored. Standard compression tests are performed after 28 d of curing, and at the time of pullout/cyclic testing. A compressive strength of 45 MPa after 28 d is expected by the supplier. This number is confirmed to be on the low side by the testing of specimens prepared during the laboratory program.

The threaded steelbars are manufactured by Dywidag, type 18WR. The material properties and bar geometry are listed in Fig. 6 and Table 1. Four anchored lengths are tested: 70 mm (= $4d_b$), 200 mm (= $11.4d_b$), 250 mm (= $14.3d_b$) and 270 mm (= $15.4d_b$). According to standards and recommendations (RILEM, 1994), a short anchored zone will represent the local bond-slip behavior. The 70 mm embedded specimens are therefore used to determine the constitutive relation between the bond stress and the anchor slip.

The rock anchors are inserted into the pre-grouted 50 mm holes in the concrete block. The grouting extends to the surface for all anchors. However, the specimens of $4d_b$ (70 mm) anchored length are isolated from the grout by a plastic pipe. The length of the plastic pipe inside the concrete block is 200 mm. Adhesion at the anchor end is avoided by use of tape. The specimen of $4d_b$ length is shown in Fig. 7.

Tensile load is applied by a hollow hydraulic Enerpack jack. The anchors are centered inside the jack and fixed in vertical direction by a nut on top of the piston. Two linear variable differential transformers (LVDTs) are utilized to measure the displacements approximately 40 mm above the concrete block inside the pedestal. A HBM C6A load cell is placed in between the piston and the fixation (nut). The oil pressure is measured by use of pressure sensors, the load is therefore measured by both the load cell and the oil pressure readings. The oil pressure is applied by use of a hydraulic Enerpack pump controlled by a flow control valve. The flow control valve is controlled by a Labview script (both for cyclic and static tests). The test set-up for cyclically loaded rock anchor is shown in Fig. 8.

Static tests are performed at a constant rate of displacement. RILEM (1994) recommended a standard load rate for specimens of length $5d_b$. This load rate is adjusted according to the anchored length (bond length) of the specimen being tested:

$$v_\delta = 0.5 d_b^2 x/5 \tag{8}$$

where v_δ is the load rate in N/s, and x is the ratio of bond length to d_b for the given specimen. The strain rate in mm/s is determined on the basis of derived peak bond stress τ_{bu} and s_1 (slip at peak bond stress). The cyclic load is applied with frequencies of 0.2–0.5 Hz depending on the load amplitude.

4. Test results

The purpose of this study is to investigate the failure mode defined by the interface between the rock anchor and the surrounding grout. The preferred failure mechanism is therefore a shear failure in the grout between the ribs. After pulling the anchors to failure, the failure mechanism is investigated. The inspection shows that the desired mechanism is achieved for all anchors, as illustrated in Fig. 9.

4.1. Static capacity

The normalized bond stresses versus displacement at anchor head for the specimens with the anchored lengths of 70 mm, 200 mm, 250 mm and 270 mm are presented in Figs. 10–13. The static curve represents an average of the observed values from at least two tests. Both a tri-linear curve approximation and the CEB (1991) bond stress–slip relationship as presented in Section 2.9

Table 1
Threaded steelbar properties.

Nominal bar diameter, d_b (mm)	Diameter at pitch, d_p (mm)	Cross-sectional area (mm^2)	Nominal mass parameter (kg/m)	Pitch (mm)	Characteristic breaking load (kN)	Yield strength (MPa)	Ultimate strength (MPa)
17.5	21	241	1.96	8	255	950	1050

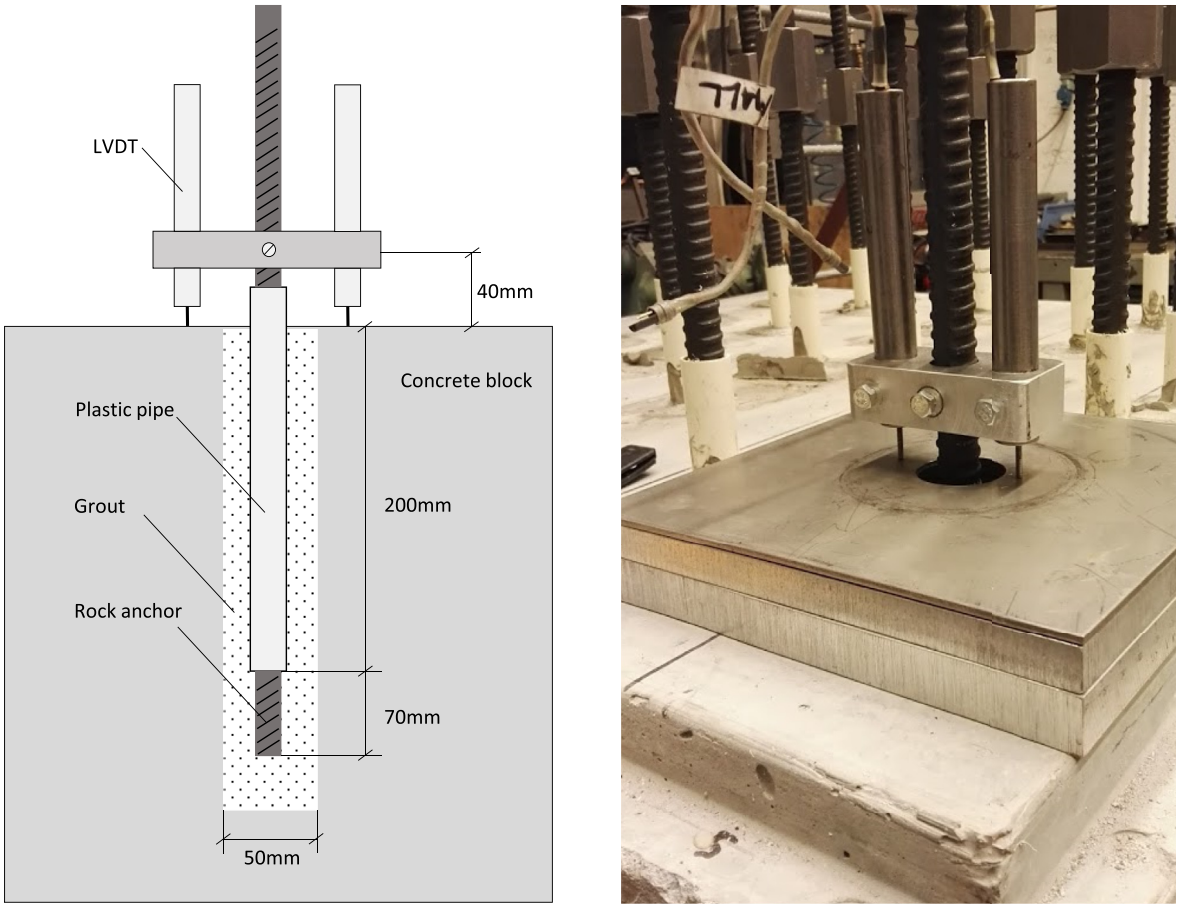

Fig. 7. Bar inserted in concrete block, $4d_b$ (70 mm) anchored length for determination of constitutive bond-slip relation. Picture at the right shows the LVDTs mounted on the bar.

are plotted together with the test results. The parameters providing best fit to the experimental data for the four anchored lengths are presented in Tables 2 and 3.

The static capacity for anchors failing under cyclic loads is estimated based on curve fitting to the normalized static bond-slip curve. These tests are of a complexity in nature, and the exact static capacity for these anchors cannot be tested. A fitting to the normalized static bond-slip curve is therefore considered to be the best approach to estimate the static capacity for these tests. This means that there is a possible deviation between the listed (Table 4) and the actual static capacities, as the latter is not known. The mean and standard deviation of static capacity for each anchored length are presented in Table 4. Statistics is based on the bearing capacities measured in the test. Cyclic tests run to failure are therefore not included in the assessment of the mean and standard deviation.

4.2. Cyclic test results

Cyclic test is performed by applying a cyclic tensile force (one-way cycling) on the anchor head. Loading is applied with minimum load preferably at $F_{min} \approx 0$. The anchor was always slightly in tension in order to avoid relaxation of the fixation of the bar. The results are interpreted to extract parameters which can be used to establish a model intended to predict slip as a function of load cycles and load size. The parameters obtained from this study can only be used to predict the capacities for similar bar dimensions and similar grout properties for anchors failing at the bar–grout interface. The methodology developed under these conditions is however expected to be valid also for other anchor dimensions failing under the same mode.

The fundamental of the model governs the relation between slip versus number of cycles (s-N diagrams), and the bond capacity as a function of slip (bond-slip diagrams). s-N relations can be found from the literature for slip values less than s_1. Relations for slip values larger than s_1 are however not found in the literature, and these relations are therefore suggested within this study.

The bond-slip curves of specimens with the anchored length of 200 mm for cycling performed at three load levels are presented in Figs. 14–16. The test performed at load level $\tau_{max\ cy}/\tau_{bu} = 0.6$ was pulled by a static load after reaching 10,000 cycles. This test indicated that the static capacity deviates less than 10% from the static tests without pre-cycling. This matches well with the publications by Rehm and Eligehausen (1979) and Oh and Kim (2007). They found that for a case where the peak load is smaller than the load corresponding to the fatigue strength of bond, a pre-applied repeated load influences bond under service load but does not adversely affect the bond near the peak strength. The static tests performed after load cycles support this conclusion.

The observed peak shear stress τ_{bu} normalized by the square root of the grout compressive strength f_c is illustrated in Figs. 17 and 18. The value along the vertical axis corresponds to the bond-factor presented in Section 2.6, recommended value ranges in 1–2.5 for deformed bars (CEB, 1991). The average bond stress is, as expected, larger for shorter anchored lengths. For longer anchored lengths, the slip will vary along the anchored zone, and at the time of failure,

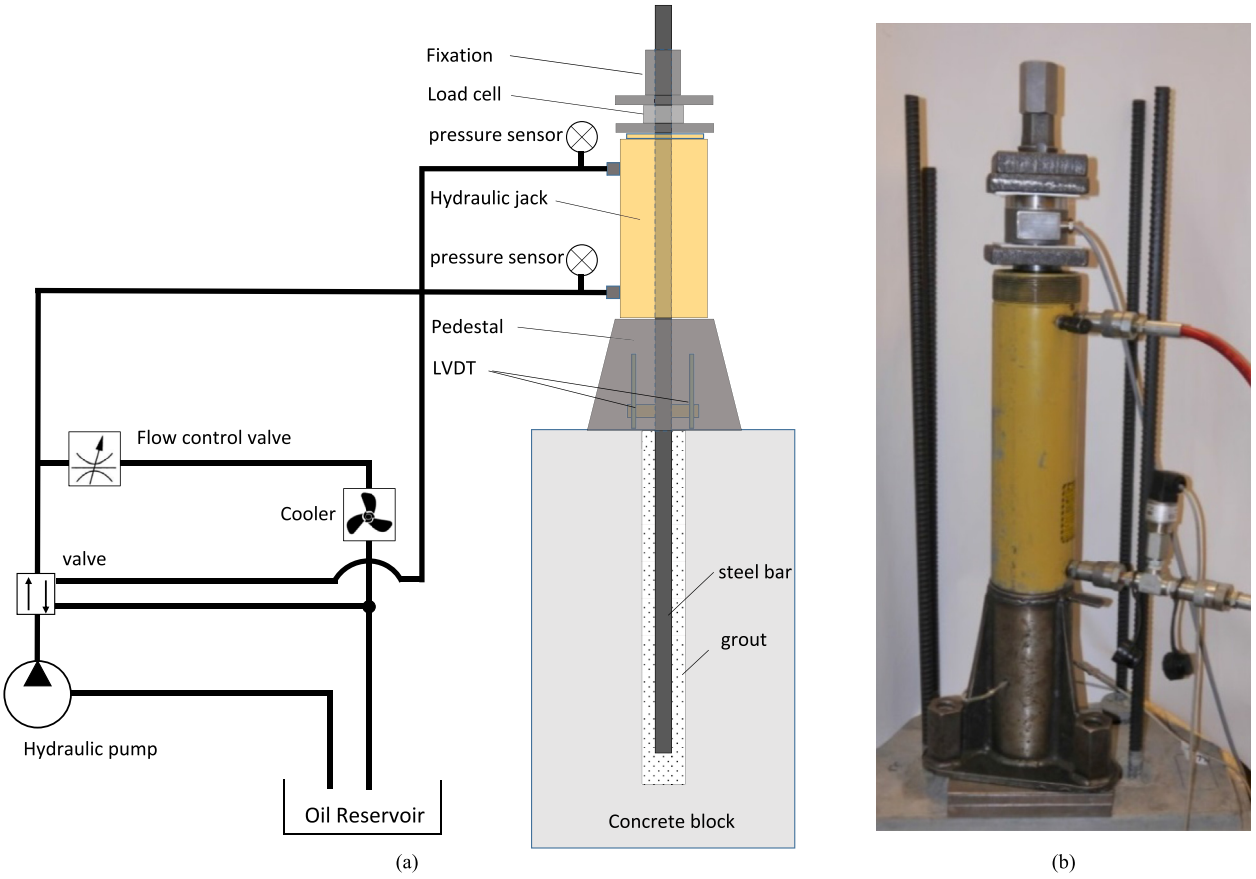

Fig. 8. Test set-up for cyclically loaded rock anchor: (a) Schematical test set-up, and (b) Picture of testing.

Fig. 9. 70 mm anchored length, pulled out after final testing. Shear failure in grout between ribs.

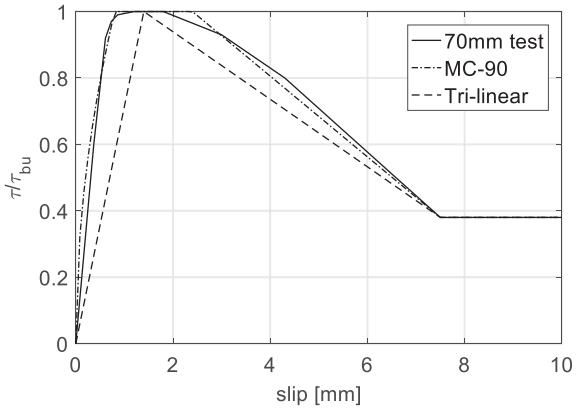

Fig. 10. 70 mm anchored length. Model code 1990 and tri-linear fit. Continuous line represents the average of three tests.

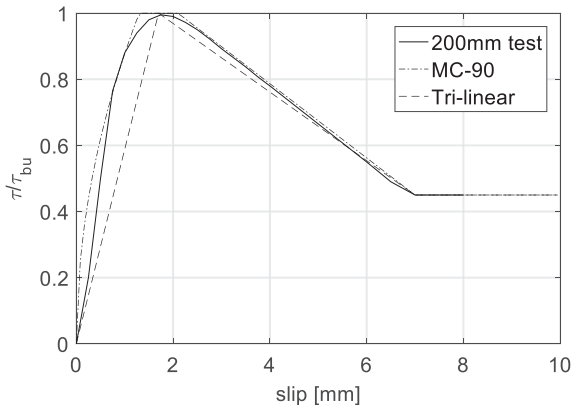

Fig. 11. 200 mm anchored length. Model code 1990 and tri-linear fit. Continuous line represents the average of two tests.

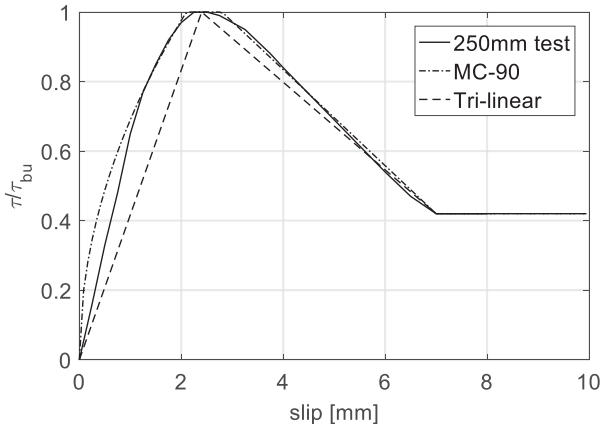

Fig. 12. 250 mm anchored length. Model code 1990 and tri-linear fit. Continuous line represents the average of two tests.

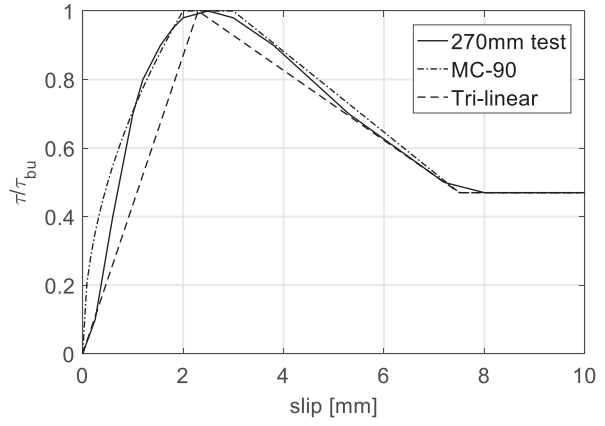

Fig. 13. 270 mm anchored length. Model code 1990 and tri-linear fit. Continuous line represents the average of two tests.

Table 2
Parameters fitted to experimental tests in the design framework of model code 1990 (CEB, 1991).

Anchored length (mm)	s_1 (mm)	s_2 (mm)	s_3 (mm)	τ_{bu} (MPa)	α	k_1	k_2	F_{max} (kN)
70	0.8	2.4	7.5	17.7	0.5		0.47	68
200	1.4	2.2	7	11.9	0.5	1.6	0.45	131
250	2.1	2.8	7	10.4	0.5	1.4	0.42	141
270	2	3	7.5	13.5	0.5	1.8	0.47	200

Note: $k_1 = \tau_{bu}/f_c^{1/2}$, and $k_2 = \tau_f/\tau_{bu}$.

the slip will be beyond s_1 for a certain partition within this zone and the bond will accordingly be lower.

The bond values are normalized by the peak bond value observed at each individual test. The normalization is performed in order to provide the model with normalized cyclic load levels. The bond capacities in absolute values are presented in Table 4.

Table 3
Tri-linear bond-slip parameters fitted to the experimental tests.

Anchored length (mm)	s_1 (mm)	s_2 (mm)	k_1	k_2	F_{max} (kN)
70	1.4	7.5	2.5	0.47	68
200	1.7	7	1.6	0.45	131
250	2.4	7	1.4	0.42	141
270	2.3	7.5	1.8	0.47	200

5. Model for rock anchors subjected to cyclic one-way loading in tension

5.1. Slip versus number of cycles

The slip development with increasing number of load cycles for a constant load level is illustrated in Fig. 19. The figure also illustrates key parameters used for the modeling of the *s-N* relationship. The "*s-N*" curve parameter s_0 is interpreted from the tests performed within this study. Slip is interpreted in terms of: (i) slip (s) measured at the maximum load amplitude and (2) residual slip (s_r) measured at the minimum load amplitude (this also applies for s_0 and s_{0r}). The slip at the maximum load amplitude will include a contribution from the elastic displacement of the bar, and possibly deformations from the test equipment. The residual slip is therefore found to be a more reliable measure to be used in the further evaluations presented in this paper. Both s and s_r as a function of N can be modeled by use of Eq. (9) and separate sets of s_0 (or s_{r0}) and b (or b_r, where b_r is equivalent to b). Eq. (9) is however valid only for slip $s < s_1$. A new model needs to be developed for $s > s_1$, this is further discussed in Section 5.2.

The cycle-dependent slip may be expressed as a function of the initial slip at the first load cycle and the number of load cycles N (Fib, 2000; Oh and Kim, 2007). The *s-N* model developed by Rehm and Eligehausen (1979) is expressed as

$$\left.\begin{aligned} s_n &= s_0(1+k_n) \\ k_n &= (1+N)^b - 1 \end{aligned}\right\} \quad (9)$$

where s_n is the slip at n cycles, s_0 is the initial slip before cyclic loading, and b is a curve fitting parameter.

According to tests performed by Oh and Kim (2007), the average b value found in their study was 0.098 for load levels at 45%, 60% and 75%. Rehm and Eligehausen (1979) reported a b value equal to 0.107, which was also adopted in model code 1990 (CEB, 1991). The power b is practically constant up to $\tau_{max\ cy}/\tau_{bu} = 0.5$ being $b = 0.119$, and it increases for higher load levels (Fib, 2000). The parameter b will in other words increase with increasing load level. Initial slip, s_0, and initial residual slip, s_{r0}, will also increase with increasing load level. Initial slip s_0, initial residual slip s_{r0}, and the curve fitting parameters b and b_r (residual) interpreted from the laboratory tests at Norwegian University of Science and Technology (NTNU) for 70 mm and 200 mm anchored lengths are presented in Table 5. Published data are also used to interpret s_0 and b values, in addition to the publication by Oh and Kim (2007) which explicitly presented s_0, s_{r0}, b and b_r. These are listed in Table 6. The bar dimension, anchored length, grout or concrete mixture will influence the magnitude of the parameters. Data achieved by testing bar dimensions corresponding to the planned anchor scale must therefore be used in a design process. The three studies found from literature used the following rebar dimensions in their experimental testing program:

(1) Rehm and Eligehausen (1979): Rebar diameter $d_b = 14$ mm, anchored length $l_b = 3d_b$;
(2) Balazs (1994): $d_b = 16$ mm, $l_b = 5d_b$; and
(3) Oh and Kim (2007): $d_b = 15$ mm, $l_b = 2d_b$.

The proposed model does not require b as an input parameter, which is calculated based on a sum of boundary conditions. This is further described in Section 5.2. Interpreted values of s_0 and s_{r0} are plotted in Figs. 20 and 21.

Table 4
Static and cyclic test results of rock bolts.

Anchored length (mm)	Test	Load level (%)[a]	Static capacity (kN)	Number of cycles to failure, N_2	τ_{bu} (MPa)[c]	$\tau_{bu}/\sqrt{f_c}$	Load period (s)	Mean (kN)	Standard deviation (kN)
70	Static	To failure	55	NA	14.3	2.02	NA	62.7	5.2
70	Static	To failure	63	NA	16.4	2.32	NA		
70	Static	To failure	69	NA	17.9	2.3	NA		
70	Cyclic	48	66[b]	NA	17.1	2.4	2		
70	Cyclic	66	55[b]	NA	14.3	2	2		
70	Cyclic	72	68[b]	NA	17.7	2.5	2		
70	Cyclic	75	56	2400	14.8	2.1	2		
70	Cyclic	76	61	1150	15.9	2.2	2		
70	Cyclic	74	68	100	17.7	2.5	2		
70	Cyclic	85	60	80	15.6	2.2	2		
70	Cyclic	83	67	60	17.4	2.5	7		
70	Cyclic	93	65	19	16.9	2.4	7		
70	Cyclic	96	70	9	18.2	2.6	7		
200	Static	To failure	138	NA	12.6	1.7	NA	131.7	5.9
200	Static	To failure	144	NA	11.3	1.5	NA		
200	Cyclic	60	133[b]	NA	12.1	1.6	3, 4		
200	Cyclic	72	125	600	10.9	1.5	10		
200	Cyclic	90	123	8	10.9	1.5	20		
200	Cyclic	94	135	4	12.3	1.7	20		
250	Static	To failure	138	NA	10	1.4	NA	138.4	6.5
250	Static	To failure	144	NA	10.5	1.4	NA		
250	Cyclic	60	142[b]	NA	10.3	1.4	3		
250	Cyclic	80	142[b]	NA	10.3	1.4	4		
270	Static	To failure	197	NA	13.3	1.8	NA	198.5	7.1
270	Static	To failure	200	NA	13.5	1.8	NA		
270	Cyclic	73	185	1480	12.5	1.7	5		
270	Cyclic	82	190	116	12.8	1.7	6		
270	Cyclic	90	205	56	13.8	1.9	7		

[a] Static capacity = 100%.
[b] Static test performed after cyclic loading history.
[c] Averaged shear stress along anchored length at the maximum force.

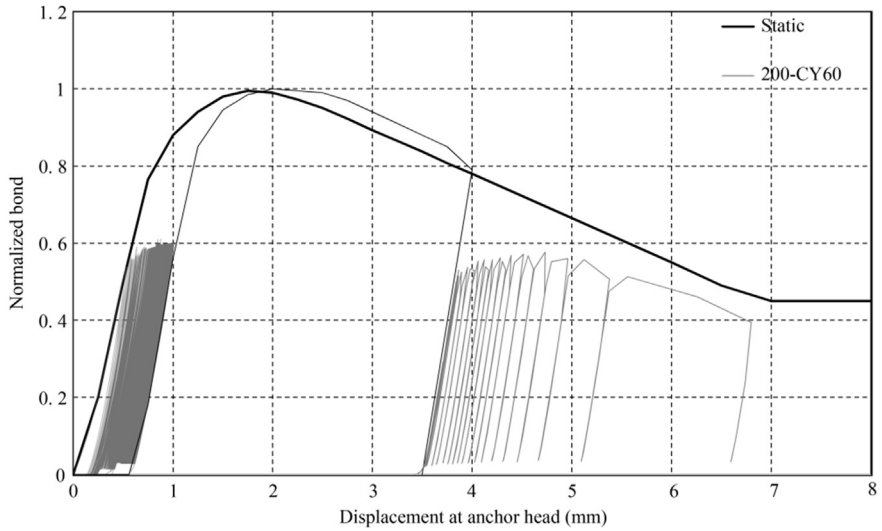

Fig. 14. Cyclic tests at $\tau_{max\ cy}/\tau_{bu} = 0.6$, 200 mm anchored length. $N = 10{,}000$ cycles.

A calculation model must accommodate load histories with varying load magnitudes. According to the findings in this study and published data, the value of initial slip (s_0) will vary with the load level $\tau_{max\ cy}/\tau_{bu}$. The relations between load level and initial slip s_0 and residual slip s_{r0} are determined experimentally and expressed by Eqs. (10) and (11) for 70 mm and 200 mm bond lengths, respectively. The model curves are included in Figs. 20 and 21 where the latter presents residual values only. A linear fit might be appropriate for low $\tau_{max\ cy}/\tau_{bu}$. The irreversible displacements seem however to increase rapidly for higher stress ratios, thus a polynomial function is suggested to model the s_{r0}-($\tau_{max\ cy}/\tau_{bu}$) relation. The curve should approach zero slip when $\tau_{max\ cy}/\tau_{bu} = 0$.

$$s_{r0} = 0.03\frac{\tau_{max}}{\tau_{bu}} + 0.2\left(\frac{\tau_{max}}{\tau_{bu}}\right)^{5} \quad \text{(70 mm anchored length)} \qquad (10)$$

$$s_{r0} = 0.17\frac{\tau_{max}}{\tau_{bu}} + 0.6\left(\frac{\tau_{max}}{\tau_{bu}}\right)^{13} \quad \text{(200 mm bond length)} \qquad (11)$$

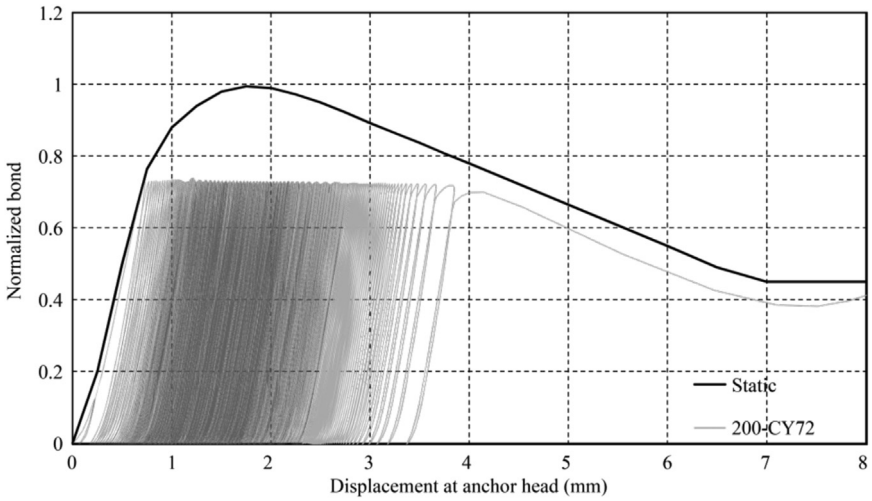

Fig. 15. Cyclic tests at $\tau_{max\ cy}/\tau_{bu} = 0.72$, 200 mm anchored length. $N = 600$ cycles.

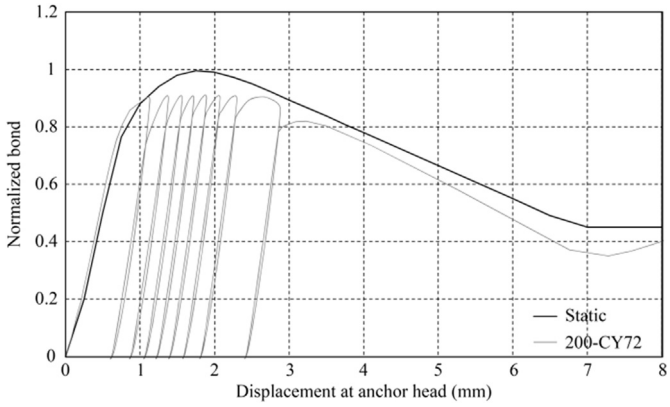

Fig. 16. Cyclic tests at $\tau_{max\ cy}/\tau_{bu} = 0.9$, 200 mm anchored length. $N = 8$ cycles.

5.2. Rate of cycles per slip

The model shall be capable of calculating the rock anchor response to cyclic load history in terms of displacement and capacity. The model shall therefore be able to determine the rate of slip based on the current "state" (slip). The rate of cycles per slip (dN/ds), or the inverse, i.e. the rate of slip per load cycle (ds/dN) as a function of load level must therefore be an input to the model. The s-N relation presented in Section 5.1 is used as a basis to develop a state-dependent resistance towards slip as a function of the load level.

Laboratory test results for specimens with the anchored lengths of 70 mm and 200 mm are used to develop the dN/ds relationship. The model must be generic for all load levels and current state (slip). The s-N relation is defined by two equations, where s_{r1} defines the shift. The expression for slip $s_r < s_{r1}$ is developed from the equation suggested by Rehm and Eligehausen (1979) modified with the cyclic load ratio R.

The formulation presented in Eq. (9) is the basis for the s-N relation used within this study, expressed as follows:

$$s_{rN} - s_{r0} = s_{r0}(1+N)^{b(1-R)} - s_{r0} = s_{r0}\left[(1+N)^{b(1-R)} - 1\right] \quad (s_r < s_{r1}) \tag{12}$$

where s_{r0} is interpreted from laboratory test results and discussed in Section 5.1; s_{rN} is the residual slip at the current state; the shape parameter b is dependent on the load level τ/τ_{max} and constrained by the requirement of reaching N_1 cycles at slip s_{r1}; the cyclic load

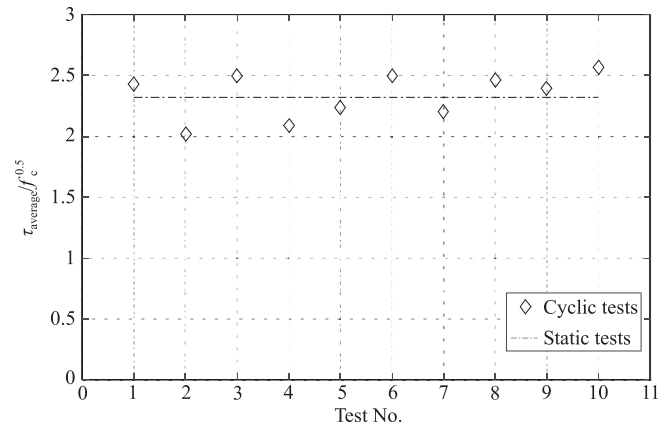

Fig. 17. Average bond stress divided by compressive strength of grout, f_c, for specimens with the anchored length of 70 mm.

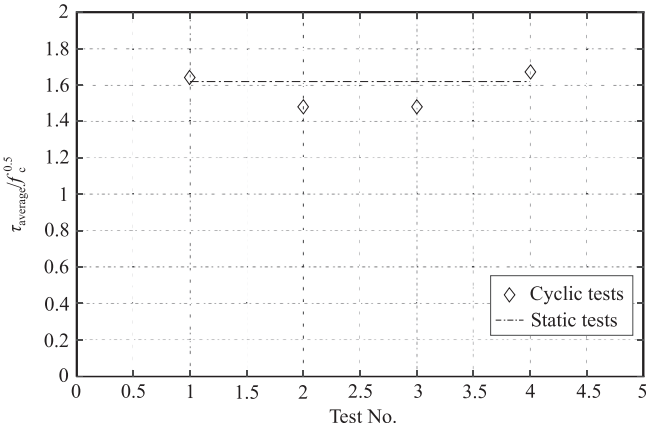

Fig. 18. Average bond stress divided by compressive strength of grout, f_c, for specimens with the anchored length of 200 mm.

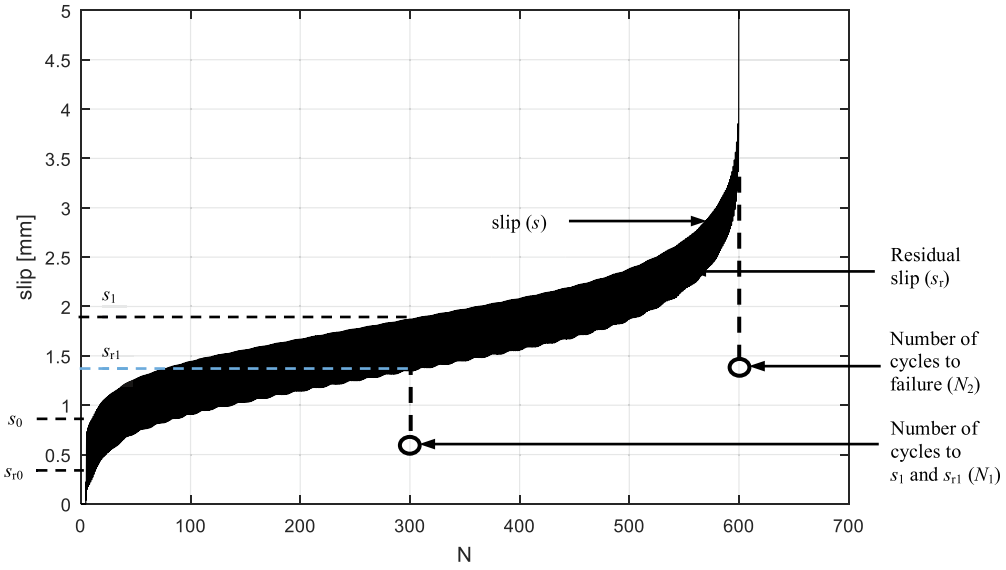

Fig. 19. *s-N* curve illustration, showing parameters for the model. d_b = 17.5 mm, 200 mm anchored length.

Table 5
"slip-*N* curve" parameters fitted to experimental tests.

Type	τ_{max}/τ_{bu}	s_{r0} (mm)	b_r	s_0 (mm)	b
NTNU-200 (d_b = 17.5 mm,	0.6	0.12	0.15	0.52	0.06
l_b = 200 mm)	0.75	0.15	0.37	0.72	0.15
	0.92	0.5	0.6	1.15	0.4
NTNU-70 (d_b = 17.5 mm,	0.35	0.01	0.06	0.24	0.31
l_b = 70 mm)	0.48	0.013	0.0225	0.25	0.14
	0.5	0.04	0.037	0.28	0.11
	0.48	0.025	0.115	0.25	0.015
	0.66	0.045	0.235	0.287	0.08
	0.72	0.032	0.3	0.5	0.046
	0.76	0.07	0.245	0.31	0.095
	0.74	0.1	0.61	0.32	0.4
	0.85	0.147	0.62	0.5	0.32
	0.83	0.12	0.66	0.5	0.34
	0.93	0.15	0.85	0.6	0.45
	0.96	0.2	0.9	0.6	0.7

ratio R is defined as the ratio of the minimum load $\tau_{min\ cy}$ to the the maximum load $\tau_{max\ cy}$ during a load cycle, i.e. $R = \tau_{min\ cy}/\tau_{max\ cy}$ ($\tau_{max\ cy} - \tau_{min\ cy}$ is the load amplitude).

Rearranging Eq. (12) to solve N and thereafter find the derivative of N with respect to $s_{rN} - s_{r0}$:

Table 6
s_0 and b values found from literature (values from Balazs et al. (1994) and Rehm and Eligehausen (1979) are interpreted).

Type	τ_{max}/τ_{bu}	s_0 (mm)	b	s_{r0} (mm)	b_r
Balazs et al. (1994)	0.2	0.007	0.1		
(d_b = 16 mm, $l_b = 5d_b$)	0.3	0.03	0.1		
	0.4	0.08	0.1		
	0.5	0.17	0.11		
	0.6	0.2	0.14		
	0.7	0.25	0.24		
	0.8	0.3	0.35		
Rehm and Eligehausen (1979)	0.4	0.027	0.07		
(d_b = 14 mm, $l_b = 3d_b$)	0.5	0.0435	0.1		
	0.65	0.095	0.1		
	0.77	0.118	0.24		
	0.85	0.325	0.45		
Oh and Kim (2007)	0.45	0.186	0.076	0.136	0.071
(d_b = 15 mm, $l_b = 2d_b$)	0.6	0.317	0.103	0.246	0.113
	0.75	0.353	0.11	0.323	0.114

$$N = \left(\frac{s_{rN}}{s_{r0}}\right)^{\frac{1}{b(1-R)}} - 1 \tag{13}$$

$$\frac{dN}{d(s_{rN} - s_{r0})} = \frac{1}{b(1-R)}\frac{1}{s_{r0}}\left(\frac{s_{rN}}{s_{r0}}\right)^{\frac{1}{b(1-R)}-1} \tag{14}$$

The *s-N* relation for slip greater than s_1 is currently not discussed in the literature. This study therefore attempts to develop this relation based on observations from the laboratory research and also published experimental work. Previous studies (e.g. Fib, 2000) divided the rate of slip into three phases for short anchored rebar under constant cyclic load amplitudes: (1) rapidly increasing rate of slip in the start of the load application, (2) constant rate of slip, and (3) increasing rate of slip leading to failure. The last phase starts when the slip reaches s_1. If s_1 is not reached, the failure phase is avoided. This progress is also apparent in Fig. 19.

The suggested relation between s_r and N for residual slip values $s_r > s_{r1}$ is expressed as.

$$s_{rN} - s_{r0} = \frac{1}{d(1 + N_2 - N)^c} - s_{r0} \quad (s_r > s_{r1}) \tag{15}$$

where N_2 is the number of cycles to failure for cyclic loading at constant $\tau_{max\ cy}/\tau_{bu}$ and constant R; and d and c are the curve fitting parameters which are dependent on the load level $\tau_{max\ cy}/\tau_{bu}$, further described in the following sections.

The model uses s_{r1} as a state parameter defining whether the *s-N* relation for $s_r < s_{r1}$ (Eq. (12)) or $s_r > s_{r1}$ (Eq. (15)) shall be used. s_{r1} is an input parameter defined by the static test and is constant for all load levels. N_1 is defined as the number of cycles at s_{r1} and N_2 is the number of load cycles until failure for a constant cyclic load level and constant R. The tests performed at NTNU did not investigate the N_2 parameter for load levels $\tau_{max\ cy}/\tau_{bu}$ lower than 0.75 as the tests were not continued beyond N = 10,000. Results found from literature (Rehm and Eligehausen, 1979; Balazs et al., 1994), together with the NTNU research are therefore used when defining an expression for N_2. It is in general found that the effect of cyclic loads (fatigue) is limited for load levels $\tau_{max\ cy}/\tau_{bu} < 0.5$.

Literature suggests that there is a strong relationship between the grout compressive strength f_c and the interface bond in the case of a deformed bar (bar with ribs or lugs). The ribs lead to a radial

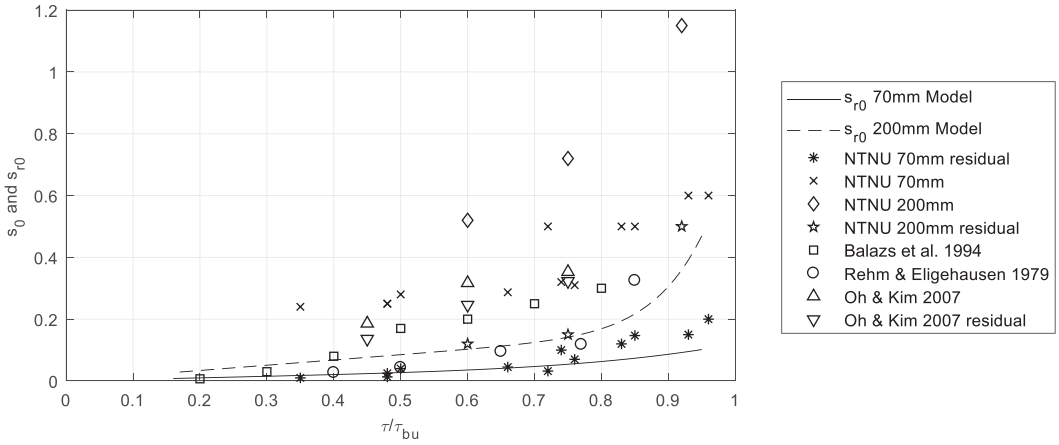

Fig. 20. Initial slip s_0 and initial residual slip s_{r0} as a function of load level. Specimens with the anchored lengths of 70 mm and 200 mm tested at NTNU, together with published data.

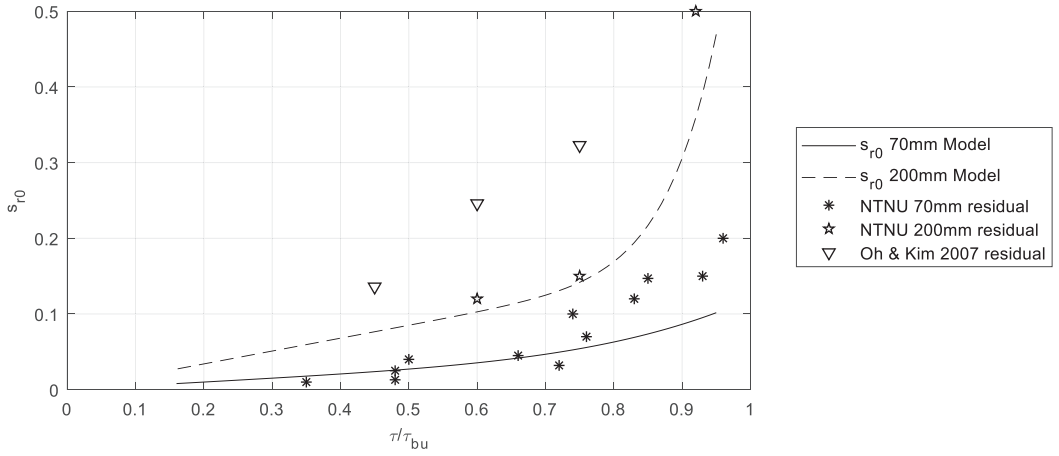

Fig. 21. Initial residual slip s_{r0} as a function of load level. Specimens with the anchored lengths of 70 mm and 200 mm tested at NTNU, together with published data.

distribution of stresses, and the bond resistance before failure is basically provided by bearing of the ribs. Therefore, the concrete compressive strength is generally considered a key parameter concerning bond. It is consequently relevant to consider *S-N* curves for concrete in this assessment (*S* is the stress). The relation defined by Aas-Jakobsen (1970), Eq. (16), is fitted to the laboratory test by the β parameter ($\beta = 0.072$ for 70 mm embedded length, and $\beta = 0.1$ for 200 mm embedded length). This model includes the $R = \tau_{\min\ cy}/\tau_{\max\ cy}$ relation, which in turn enables the model to deal with a variation of both $\tau_{\min\ cy}$ and $\tau_{\max\ cy}$.

$$N_2 = 10^{\frac{1-\tau_{\max\ cy}/\tau_{bu}}{(1-R)\beta}} \tag{16}$$

A relation presented by Stüssi in 1965 (Fib, 2000), Eq. (17), is compared to the test results. It should be noted that the original equation is modified by the introduction of the relation $R = \tau_{\min\ cy}/\tau_{\max\ cy}$. Fib (2000) presented this curve for specimens reaching 0.5 mm and 5 mm slips correspondingly. The tests were performed on specimens of $d_b = 16$ mm, $l_b = 5d_b$, and $R = 0.1$.

$$N_2 = \left(\frac{k_0 - \frac{\tau_{\max\ cy}}{\tau_{bu}}}{\frac{\tau_{\max\ cy}}{\tau_{bu}}k_3 - k_1}\right)^{\frac{1}{k_2(1-R)}} \tag{17}$$

The N_2-($\tau_{\max\ cy}/\tau_{bu}$) expression suggested by Aas-Jakobsen (1970) (Eq. (16)) is further used within this study. This expression is preferred due to the relatively simple expression, and because it is a well-accepted formulation for concrete fatigue life. Another argument is that the Stüssi formulation (Eq. (17)) may predict an infinite number of cycles until failure for low load levels, given the values of the parameters k_0, k_1, k_2 and k_3. This may be correct, nevertheless, infinite numbers would complicate the calculation model. The N_2 curve is plotted as a function of load level and presented in Fig. 22 together with the test results.

The number of cycles required to reach residual slip (N_1) is assessed based on laboratory results at NTNU and published experimental data. In general, the observations reveal an increasing N_1/N_2 ratio with decreasing cyclic load level $\tau_{\max\ cy}/\tau_{bu}$. N_1 is expressed as follows and included in Fig. 22:

$$N_1 = 0.27N_2\frac{\tau_{\max\ cy}}{\tau_{bu}} + 0.73N_2\left(1 - \frac{\tau_{\max\ cy}}{\tau_{bu}}\right) \tag{18}$$

The combination of Eqs. (12) and (15) shall describe the complete slip behavior for $0 < N < N_2$. Both equations shall be equal to s_{r1} for $N = N_1$, this boundary condition is expressed as

$$s_{r0}\left[(1+N_1)^{b(1-R)} - 1\right] = \frac{1}{d(1+N_2-N_1)^c} - s_{r0} \tag{19}$$

This boundary condition is used to define b by rearranging Eq. (19):

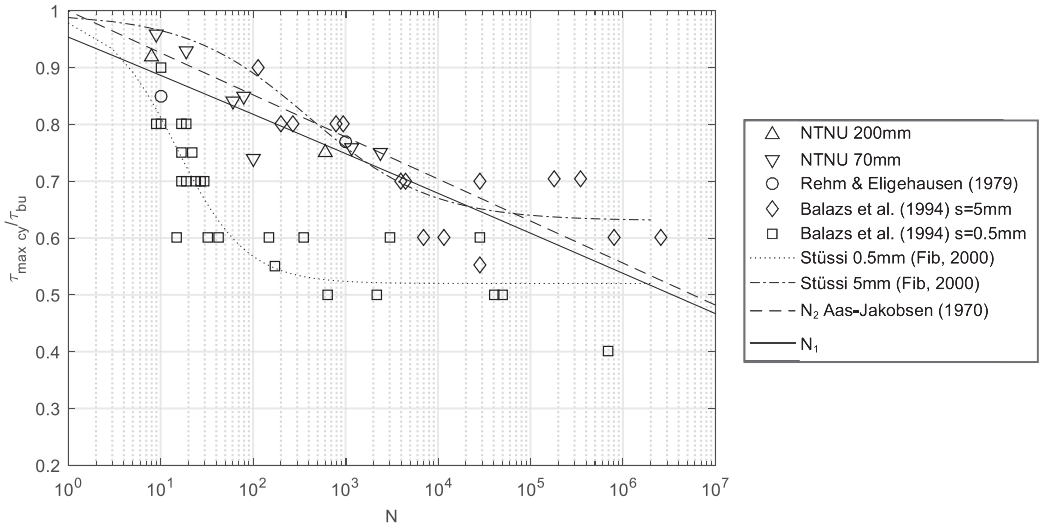

Fig. 22. N_2 as a function of load level $\tau_{\max\,cy}/\tau_{bu}$ at $R = 0$.

$$b = \frac{\ln(s_{r1}/s_{r0})}{(1-R)\ln N_1} \tag{20}$$

The parameter b can thereby be calculated by the model, and thus is not required as an input. The requirement of equal slip per cycle at s_{r1} is another boundary condition. The derivatives of Eqs. (12) and (15) with respect to N are as follows:

$$\frac{\mathrm{d}(s_{rN}-s_{r0})}{\mathrm{d}N} = b(1-R)s_{r0}(1+N)^{b(1-R)-1} \quad (s_r < s_{r1}) \tag{21}$$

$$\frac{\mathrm{d}(s_{rN}-s_{r0})}{\mathrm{d}N} = \frac{c}{d}(1+N_2-N)^{-c-1} \quad (s_r > s_{r1}) \tag{22}$$

The parameters c and d can be solved analytically by applying the boundary condition that $\mathrm{d}s_r/\mathrm{d}N$ for $0 < N < N_1$ is equal to $\mathrm{d}s_r/\mathrm{d}N$ for $N_1 < N < N_2$ when $N = N_1$. First by solving d from Eqs. (21) and (22), and subsequently solving c by substituting d into Eq. (19), we have

$$d = \frac{c}{b(1-R)s_{r0}}(1+N_2-N_1)^{-c-1}(1+N_1)^{1-b(1-R)} \tag{23}$$

$$c = \frac{b(1-R)(1+N_2-N_1)}{1+N_1} \tag{24}$$

The model shall be either displacement controlled or force controlled (input in terms of displacement increments or load increments). The derivative of Eq. (12) with respect to s_r is defined by Eq. (14), and the derivative of Eq. (15) with respect to residual slip s_r is defined as

$$\frac{\mathrm{d}N}{\mathrm{d}(s_{rN}-s_{r0})} = \frac{d}{c}(1+N_2-N)^{c+1} \quad (s_r > s_{r1}) \tag{25}$$

The laboratory test results from rock bolts of 70 mm and 200 mm anchored lengths are used to test and validate the rate of slip relations. The results are shown in Figs. 23–26. Figs. 23 and 25 present the $\mathrm{d}N/\mathrm{d}s$ relation established by use of Eqs. (14) and (25) compared to laboratory results, respectively. Fig. 26 presents the result obtained by integrating the $\mathrm{d}N/\mathrm{d}s$ relation (slip versus N),

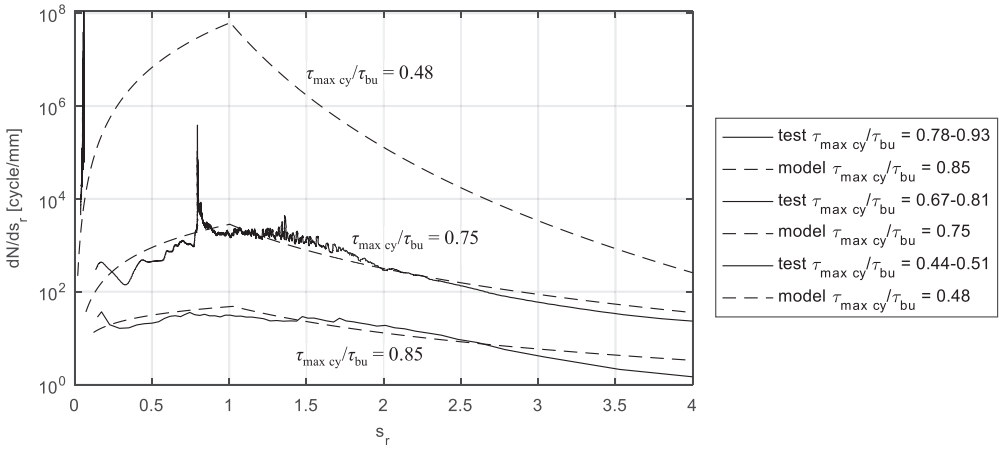

Fig. 23. Rate of cycles per slip ($\mathrm{d}N/\mathrm{d}s_r$) versus residual slip ($s_r$) at anchor head for load levels $\tau_{\max\,cy}/\tau_{bu} = 0.85$, 0.75 and 0.48 for 70 mm anchored length.

compared with the laboratory result. The model curve for s_{r0} presented in Eq. (10) is used in the assessment.

The legend indicates the best fit cyclic load ratio $\tau_{max\ cy}/\tau_{bu}$ for the laboratory tests ($\pm\sigma$, where σ is the standard deviation). This presentation is preferred due to the uncertainty with respect to the static capacity. Further, the model-legend presents the $\tau_{max\ cy}/\tau_{bu}$ providing the best fit to the test results.

The expression for N_2 was adjusted to fit the 200 mm embedded anchors, while the N_1 expression (Eq. (18)) was kept the same. The initial residual slip s_{r0} used in the back calculations is expressed by Eqs. (10) and (11).

5.3. Validation of the model

The model is developed and checked for constant cyclic load levels. The model shall nevertheless work for a variety of load intensities. A verification should therefore include back calculation of an anchor subjected to a load history including variations of cyclic load intensity. Anchors of two different embedded lengths are tested under displacement control (200 mm bond length) and load control (70 mm bond length). Both tests are performed with the intention to be used for verification of the model.

5.3.1. Displacement controlled test, 200 mm bond length

The maximum displacement (s_0 at maximum load amplitude) is kept constant. The displacement is controlled manually by decreasing the load level to maintain a constant deformation.

Applied load $\tau_{max\ cy}/\tau_{bu}$ versus residual slip is presented in Fig. 27, and $\tau_{max\ cy}/\tau_{bu}$ versus number of cycles N is presented in Fig. 28. Calculation of N_2 is performed by the Aas-Jakobsen formulation (Eq. (16)) with $\beta = 0.1$. The description of initial residual slip is identical to Eq. (11).

The back calculation is performed by using the dN/ds formulation described in Eq. (14) ($s_r < s_{r1}$). The script iterates with increasing slip increments ds_r:

$$s_{ri} = s_{r(i-1)} + \mathrm{d}s_r \tag{26}$$

The dN/ds_r increment is described by Eqs. (14) and (25). The accumulated number of cycles is thereafter summarized as

$$N_i = N_{i-1} + \frac{\mathrm{d}N}{\mathrm{d}s_r}\mathrm{d}s_r \tag{27}$$

The current load level, $\tau_{max\ cy}/\tau_{bu}$, is thereafter determined by an equation fitted to the ($\tau_{max\ cy}/\tau_{bu}$)-N curve resulting from the displacement controlled test described as follows:

$$\left(\tau_{max\ cy}/\tau_{bu}\right)_i = 0.8N_i^{-0.1} \tag{28}$$

The back calculation is performed by an explicit routine. The sensitivity is checked by varying the step size until the variation in the calculated result is insignificant. The back calculated result is compared with the laboratory test result and presented in Fig. 29 (the laboratory test result is presented with diamond symbols in

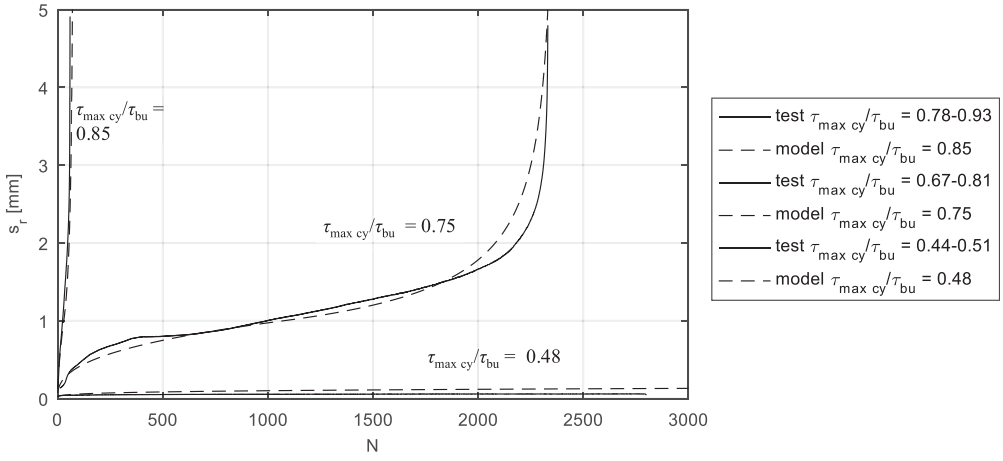

Fig. 24. s_r-N curves for 70 mm anchored length, laboratory test results together with back calculated values using the model.

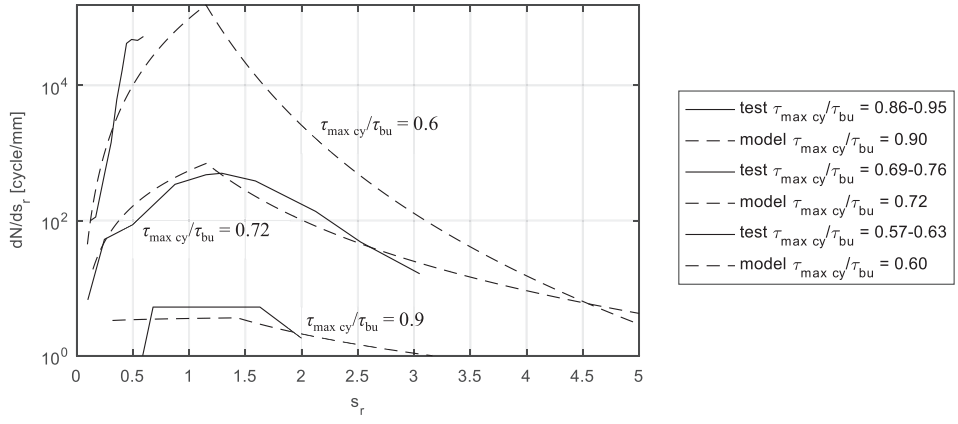

Fig. 25. Rate of cycles per slip (dN/ds_r) versus residual slip (s_r) at anchor head for load levels $\tau_{max\ cy}/\tau_{bu}$ = 0.9, 0.72 and 0.6 for 200 mm anchored length.

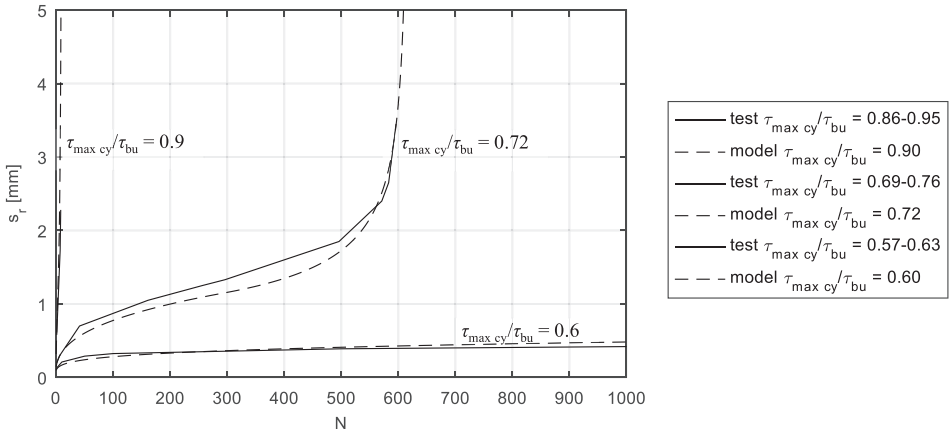

Fig. 26. Number of cycles versus residual displacement at anchor head. Modeling results compared with laboratory testing values for 200 mm anchored length.

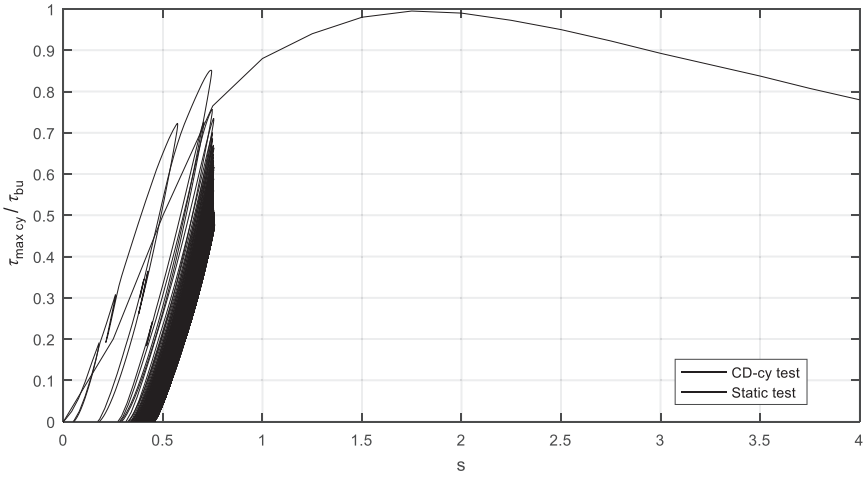

Fig. 27. Slip versus cyclic load level curves obtained from displacement controlled tests on specimens with the anchored length of 200 mm.

the figure, i.e. no line). The figure illustrates the back calculation result using two different approaches:

(1) back calculation by use of state-dependent rate of slip, dN/ds, illustrated by continuous line in Fig. 29; and
(2) back calculation by use of a constant load level, $\tau_{max\ cy}/\tau_{bu} = 0.5$ and 0.6, illustrated by dotted lines in Fig. 29.

5.3.2. Load controlled test, 70 mm embedment

The load controlled tests are performed by applying constant load levels in parcels of N cycles. The load parcels are applied sequentially with increasing load intensity and constant cyclic loading period. The load is applied with $\tau_{min\ cy}$ approximately equal to zero. The Aas-Jakobsen formulation (Eq. (16)) is used to define N_2 with $\beta = 0.072$. The residual slip is expressed by Eq. (10).

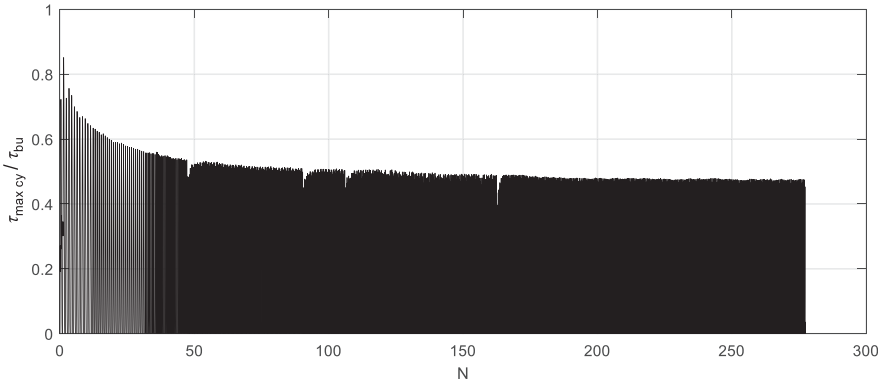

Fig. 28. Number of cycles versus cyclic load level curve obtained from displacement controlled tests on specimen with the anchored length of 200 mm.

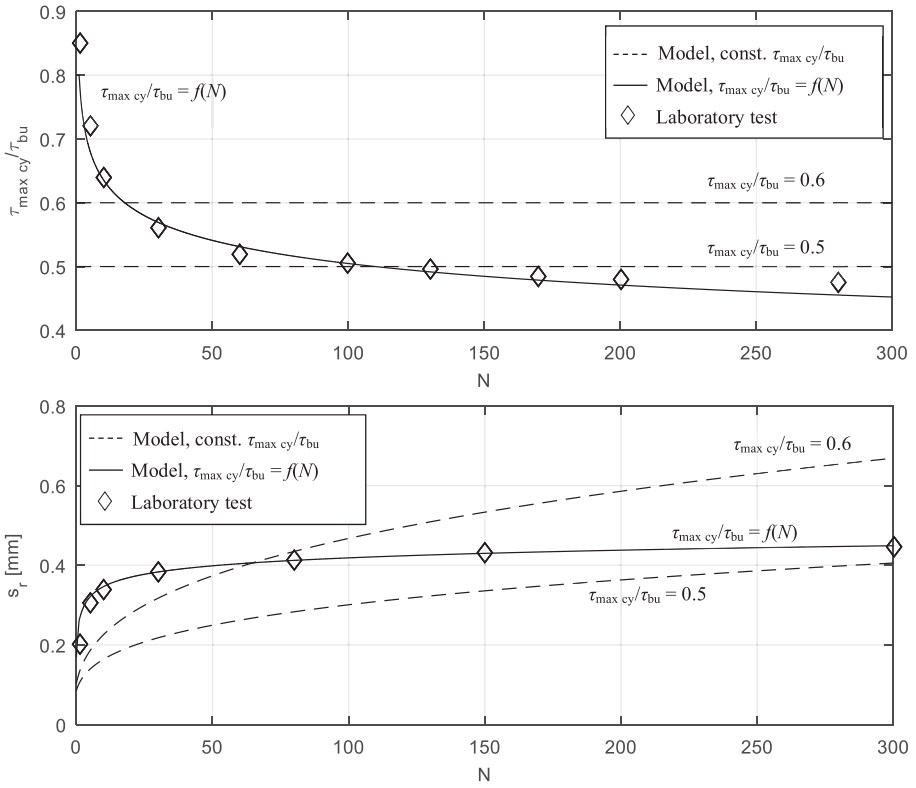

Fig. 29. Back calculation result. Laboratory test indicated by diamonds. Iterative procedure using state-dependent parameters shown by continuous line, constant $\tau_{max\ cy}/\tau_{bu} = 0.5$ and 0.6 shown by dotted lines.

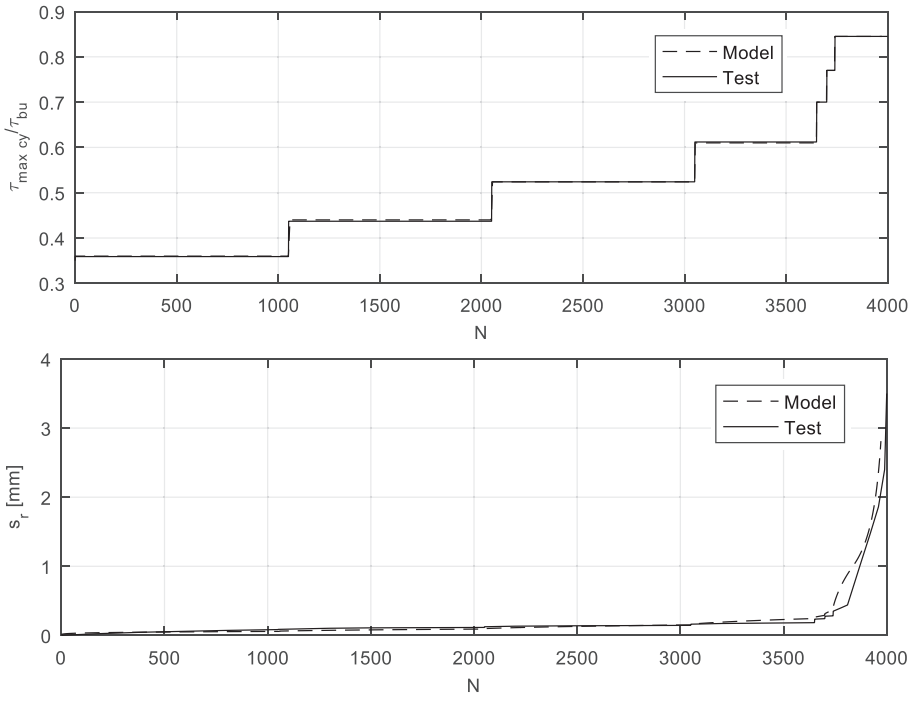

Fig. 30. Back calculation of load controlled laboratory test. Load history presented in the upper figure, and the calculated slip-*N* curve compared with the observed result presented in the lower figure.

Table 7
Model input parameters.

Parameter	Description
$s_{r0} = f(\tau_{max}/\tau_{bu})$	Initial residual slip (Eq. (10)), alternatively use s_0. s_{r0} is a function of cyclic load level
s_{r1}	Residual slip at ultimate bond stress (τ_{bu}), constant for all load levels
β	Defining number of cycles to failure, N_2 (Eq. (16)). Constant for all load levels

Table 8
Load input parameters.

Parameter	Description
$\tau_{max\ cy}/\tau_{bu}$	Cyclic load level, where $\tau_{max\ cy}$ is the maximum load during a load cycle, and τ_{bu} is the ultimate (or peak) bond strength
N	Number of load cycles
$R = \tau_{min\ cy}/\tau_{max\ cy}$	$\tau_{min\ cy}$ is the minimum load, and $\tau_{max\ cy}-\tau_{min\ cy}$ is the load amplitude

Fig. 30 presents the load history applied to the rock anchor in terms of $\tau_{max\ cy}/\tau_{bu}$ versus number of load cycles, and the resulting residual slip versus number of cycles.

6. Conclusions and recommendations

Bond strength versus slip development for rock anchors exposed to cyclic loading is investigated within this study. Different lengths of anchored (bonded) zone, i.e. $4d_b$, $11.4d_b$, $14.3d_b$ and $15.4d_b$, are applied in the study. According to standards and recommendations (RILEM, 1994), anchored zone of $4d_b$ will represent local bond-slip behavior. The study therefore investigates both the constitutive relation between the bond stress versus slip and the characteristics of pullout capacity for anchors with longer bond zones subjected to cyclic loading.

For a relatively long anchor, the local slip will vary along the anchored length. The experimental and theoretical researches presented within this paper may thus be used in a numerical model to calculate the complete rock anchor capacity after a cyclic load history.

The model input parameters must be defined by static and cyclic tests in laboratory or field. The required parameters are presented in Table 7. The load input may be provided in terms of a random load history. The model supports the load history format presented in Table 8.

The following conclusions summarize the findings from this study:

(1) The literature study concludes that the maximum bond strength is not reduced as long as the displacement caused by cyclic loading is lower than the displacement (s_1) at the peak stress for the static curve (Rehm and Eligehausen, 1979; Oh and Kim, 2007). The tests presented in this study determines also that the rock anchor will not necessarily fail after exceeding the displacement at the peak bond, but the maximum capacity will be reduced according to the bond-slip (bond-displacement) diagram.

(2) The static bond-slip relation found from the tests can be modeled by use of model code 1990 (CEB, 1991), or a tri-linear model as suggested by Benmokrane et al. (1995b). Model code 90 produces a better match to the laboratory result, nevertheless the tri-linear model might be easier to be implemented in a numerical model.

(3) The relation between the number of load cycles to failure as a function of load level proposed by Oh and Kim (2007) is only valid if one assumes failure at s_1 (displacement at the peak stress). The experimental study presented herein shows however that significant number of cycles can be applied also beyond s_1 (depending on the load level). There is therefore a relatively large safety margin for low load levels. The margin will however decrease with increasing load level. The assumption that bond failure occurs when the slip value under repeated loading reaches the slip s_1 (Oh and Kim, 2007) is therefore correct if the maximum load is applied, but may be regarded to be on the conservative side for lower load levels.

(4) Literature shows that for an anchor subjected to cyclic loading at constant load amplitude, the rate of cycles per slip (dN/ds) is rapidly increasing at the beginning, followed by a somewhat constant dN/ds until s_1 is reached. After reaching s_1, dN/ds increases until failure is reached. The laboratory results and back calculations presented within this study show that the dN/ds (or the inverse, ds/dN) may be modeled by use of two formulations: one for slip $s < s_1$ and the other for $s > s_1$. The model for $s < s_1$ is found from literature, whereas the model for $s > s_1$ is developed based on this study and published experimental research. A complete model expressing the dN/ds development with slip is by these means suggested within this paper.

(5) Ultimate bond strength, τ_{bu}, may be expressed as a function of compressive strength of grout, $\tau_{bu} = a\sqrt{f_c}$, where a might vary from 1.5 to 2.5 according to model code 1990 (CEB, 1991). The tests presented herein reveal $a = 2$–2.5 for 70 mm anchored length.

(6) The combination of creep and cyclic induced slip is not tested in this study. When the cyclic load approaches a certain load period, creep induced slip will add to the measured slip. If the loading period increases, measured dN/ds might decrease (or inversely, ds/dN will increase). Literature suggests that creep effect is negligible for frequencies between 1 Hz and 10 Hz (Zhang et al., 1996). The tests within this study are performed with frequencies of 0.1–0.5 Hz. Measured slip most likely includes some degree of creep displacements. Zhang et al. (1996) presented an equation including the cyclic load level $\tau_{max\ cy}/\tau_{bu}$, $R\ (=\tau_{min\ cy}/\tau_{max\ cy})$, f (frequency) and N (number of cycles). The relation is an extension of the S-N relation for plain concrete presented by Aas-Jakobsen (1970). Creep effects will lead to a reduced N_2 value. The model can be extended by including the equation by Zhang et al. (1996), and thereby reduce N_2 with reduced loading frequency. More tests will however be required to better define the parameters required for this model. Long-term creep (years) or relaxation should also be considered in a final model.

(7) A trend of decreasing frictional capacity with increasing slip is observed. This effect is however not studied in detail. The rate of decrease is larger than the decrease caused by the reduced bar length inside the concrete. This might be caused by crushing of particles along the interface, and at the same time by a reduced degree of confinement. This might be worthwhile to be noticed, as the residual strength after failure will be one of the ingredients in a complete numerical model.

(8) The formulations presented herein are intended to be used for short incremental lengths along the embedded length of a rock anchor. “Short” means a length short enough to ensure that the relative displacement between the bar and the grout is constant within the anchored zone. The total capacity of a

rock anchor will be modeled by a number of increments in a displacement-compatible model. The tests performed on anchors with 200 mm anchored length show conversely that the model also can be used as a "macro-model" describing the total behavior of a longer embedded anchor or rock bolt as well.

(9) The test results show a somewhat large spread in number of cycles until failure, N_2. Fig. 22 presents the observed N_2 values for tests performed at constant load amplitudes including published results. The model comprises a formulation for N_2, and this formulation should represent the average of the observed values. This might nevertheless lead to a poor match for back calculation of short increments of a rock anchor but should be representative for a rock anchor consisting of several increments constituting the complete length of an anchor.

(10) N_2 defined by Eq. (16) may be the most appropriate equation to be implemented in the model. This formulation contains few factors and is continuous in the complete range of $\tau_{\max\ cy}/\tau_{bu} = 0–1$. The alternative formulation (Eq. (17)) may also be used.

(11) Design factors are not discussed herein as the purpose of this work is to investigate and model the characteristic bond-slip development for passive rock anchors subjected to cyclic loads. However, if a design factor should be applied, it could be appropriate to factorize the N_2 parameter by a design factor, and the N_2 curve should in addition be conservatively defined.

(12) Several studies are performed on cyclically loaded rebar in concrete. Rehm and Eligehausen (1979) concluded that the fatigue strength of bond corresponds to the fatigue strength of centrally loaded concrete. This means that no fatigue bond failure will occur during several million load cycles if, for the usual anchorage lengths required for reinforcing bars, the upper load is smaller than about 50% of the static pullout load. Tests performed on rock anchors also conclude that damage is not observed for cyclic load levels less than 25% of ultimate anchor capacities (Benmokrane et al., 1995a), moreover, it shall be noted that these tests were performed on anchored lengths considerably longer than 5 times the bar diameter.

Test results revealed some variations in the peak bond stresses on similar bonded lengths. The variations are probably caused by the degree of mortar infill in between the ribs and the confinement at the top of the anchor. A trend is found between the degree of infill and peak bond stress by assessing the area of infill versus no infill (after pulling out the bars). Displacements in the test rig itself might also to some extent contribute to the variations in the results. The variations decrease with increasing anchored lengths. This might indicate that a short length is more sensitive with respect to variabilities in the test set-up and installation of the anchors (e.g. voids in grout).

Published results also reveal somewhat varying test results for similar test conditions (e.g. Fig. 22). Variations might be caused by the nature of the materials being tested, increasing number of tests will however improve the basis for determination of model parameters.

It is emphasized that the results in terms of capacities and deformations are representative for the bar dimensions and material properties included within this test only. The model characteristics should nevertheless be considered generic as long as the failure mode is located at the bar–grout interface.

The limitations with respect to creep and time effects as commented in Section 6 (and Sections 2.2 and 2.3) must be noticed. Cyclic tests are performed in the range of 0.14–0.5 Hz. The importance of effects caused by cyclic loads outside this range should be addressed.

Conflicts of interest

The authors wish to confirm that there are no known conflicts of interest associated with this publication and there has been no significant financial support for this work that could have influenced its outcome.

Acknowledgements

The study is sponsored by the Norwegian Public Roads Administration (NPRA). The work is part of the research program initiated by NPRA associated with the E39 coastal highway route along the west coast of Norway.

The work performed by master students Egil A. Behrens and Håvard O. Hagen is highly appreciated. The experimental work presented here is assisted by these two students throughout the work with their master theses.

References

Aas-Jakobsen K. Fatigue of concrete beams and columns. Trondheim, Norway: Institutt for Betongkonstruksjoner, NTH; 1970.

ACI. An abstract: state-of-the-art report: bond under cyclic loads. Reapproved edition. ACI Committee 1999;408.

American Concrete Institute (ACI). State-of-the-art report: bond under cyclic loads. ACI Committee 1992;408.

Balazs GL, Koch R, Harre W. Verbund von Stähl in Beton unter Betriebsbeanspruchung. In: Deutcher Ausschuss für Stahlbeton-30. Stuttgart: Forschungskolloquium; 1994. p. 167–76 (in Germany).

Ballivy G, Benmokrane B, Sage AP, Saioudi A. Stabilisation des talus rocheux à l'aide d'ancrages injectés: influence des chargements cycliques. In: Bonnard C, editor. Proceedings of the 5th international symposium on landslides. Rotterdam, Netherlands: A.A. Balkema; 1988. p. 839–46 (in French).

Benmokrane B, Ballivy G. Five-year monitoring of load losses on prestressed cement-grouted rock anchors. Canadian Geotechnical Journal 1991;28(5):668–77.

Benmokrane B, Chekired M, Xu H, Ballivy G. Behavior of grouted anchors subjected to repeated loadings in field. Journal of Geotechnical Engineering 1995a;121(5):413–20.

Benmokrane B, Chennouf A, Mitri HS. Laboratory evaluation of cement-based grouts and grouted rock anchors. International Journal of Rock Mechanics and Mining Sciences and Geomechanics Abstracts 1995b;32(7):633–42.

Brown ET. Rock engineering design of post-tensioned anchors for dams – a review. Journal of Rock Mechanics and Geotechnical Engineering 2015;7(1):1–13.

Ciampi V, Eligehausen R, Bertero VV, Popov EP. Analytical model for deformed bar bond under generalized excitations. Stuttgart: Universitätsbibliothek der Universität Stuttgart; 1981.

Comitee Euro-International De Beton (CEB). CEB-FIP model code 1990 – design code. Thomas Telford; 1991.

Dallyn P, El-Hamalawi A, Palmeri A, Knight R. Experimental testing of grouted connections for offshore substructures: a critical review. Structures 2015;3:90–108.

Eligehausen R, Popov EP, Bertero VV. Local bond stress-slip relationships of deformed bars under generalized excitations. Stuttgart: Universitätsbibliothek der Universität Stuttgart; 1981.

Furuya N, Yamaoka R, Paulson JBC. Construction of Akashi Kaikyo bridge west anchorage. Journal of Construction Engineering and Management 1994;120(2):337–56.

Gómez J, Cadden AW, Traylor RP, Bruce DA. Connection capacity between micropiles and concrete footings: interpretation of test results and design recommendations. International Association of Foundation Drilling 2005.

Hanna TH. Foundations in tension: ground anchors. Zurich, Switzerland: Trans. Tech. Publications; 1982.

Howard T, Riley B, Upsall B, Horvitz G. Structural design of deep water pontoon mooring anchors. In: Proceedings of Ports '13: 13th Triennial international conference. American society of civil engineers (ASCE); 2013.

Hyett AJ, Bawden WF, Reichert RD. The effect of rock mass confinement on the bond strength of fully grouted cable bolts. International Journal of Rock Mechanics and Mining Sciences and Geomechanics Abstracts 1992;29(5):503–24.

International Federation for Structural Concrete (Fib). Bond of reinforcement in concrete: state-of-art report. Lausanne, Switzerland: FIB Bulletin 10, CEB-FIP; 2000.

Ivanović A, Neilson RD. Modelling of debonding along the fixed anchor length. International Journal of Rock Mechanics and Mining Sciences 2009;46(4):699–707.

Kaiser PK, Yazici S, Nose J. Effect of stress change on the bond strength of fully grouted cables. International Journal of Rock Mechanics and Mining Sciences & Geomechanics Abstracts 1992;29(3):293–306.

Kim KT, Song CY, Shin YS. Yi Sun-sin Bridge: construction of two different anchorage systems. In: Proceedings of the 18th IABSE congress. Seoul, Korea; 2012. p. 248–57.

Kılıc A, Yasar E, Celik AG. Effect of grout properties on the pull-out load capacity of fully grouted rock bolt. Tunnelling and Underground Space Technology 2002;17(4):355–62.
Kılıc A, Yasar E, Atis CD. Effect of bar shape on the pull-out capacity of fully-grouted rockbolts. Tunnelling and Underground Space Technology 2003;18(1):1–6.
Lotsberg I, Serednicki A, Cramer E, Bertnes HK, Haahr PE. On the structural capacity of grouted connections in offshore structures. In: Jan Vugts symposium on design methodology of offshore structures. American Society of Mechanical Engineers (ASME); 2011. p. 667–77.
Ma S, Zhao Z, Nie W, Gui Y. A numerical model of fully grouted bolts considering the tri-linear shear bond–slip model. Tunnelling and Underground Space Technology 2016;54:73–80.
Norwegian Public Roads Administration (NPRA). Hardanger bridge technical brochure. NPRA 2013.
Oh BH, Kim SH. Realistic models for local bond stress-slip of reinforced concrete under repeated loading. Journal of Structural Engineering 2007;133(2):216–24.
Rehm G, Eligehausen R. Bond of ribbed bars under high cycle repeated loads. Journal of the American Concrete Institute 1979;76(2):297–309.
International Union of Laboratories and Experts in Construction Materials, Systems and Structures (RILEM). RILEM technical recommendations for the testing and use of construction materials. London: E & FN Spon; 1994.
Verderame GM, Ricci P, Carlo GD, Manfredi G. Cyclic bond behaviour of plain bars. Part I: experimental investigation. Construction and Building Materials 2009a;23(12):3499–511.
Verderame GM, De Carlo G, Ricci P, Fabbrocino G. Cyclic bond behaviour of plain bars. Part II: Analytical investigation. Construction and Building Materials 2009b;23(12):3512–22.
Yahia A, Khayat KH, Benmokrane B. Evaluation of cement grouts for embedding anchors under water. Materials and Structures 1998;31(4):267–74.
Yazici S, Kaiser PK. Bond strength of grouted cable bolts. International Journal of Rock Mechanics and Mining Sciences & Geomechanics Abstracts 1992;29(3):279–92.
Zhang B, Phillips DV, Wu K. Effects of loading frequency and stress reversal on fatigue life of plain concrete. Magazine of Concrete Research 1996;48:361–75.

Joar Tistel is a senior geotechnical engineer with 13 years of experience. He is currently undertaking a PhD study at the Norwegian University of Science and Technology. The topic of this work is “Bridge foundations at large water depths”. His experience ranges from traditional geotechnical problems, to advanced geotechnical analysis, both onshore and offshore. He holds a broad experience from offshore foundation engineering within the energy sector (oil & gas, and renewable). His key expertise relates to gravity based structures (GBS), jackets, subsea structures resting on suction piles and mudmats, foundations for offshore wind turbines, and dry docks for large offshore structures. He has been working on several international projects as geotechnical lead engineer during 13 years as an employee within the Norwegian consultancy company Multiconsult. He has also participated in work with standards and guidelines. He was the key responsible for the update of the foundations section within the Document ACI 357R-84 “Guide for the design and construction of fixed offshore concrete structures” (American Concrete Institute). He is a committee member of ACI 357.